Liu et al. *Zool. Res.* 2021, 42(3): 287−293
https://doi.org/10.24272/j.issn.2095-8137.2020.318

ZR | Zoological Research

Letters to the editor Open Access

Does the Dzungarian racerunner (*Eremias dzungarica* Orlova, Poyarkov, Chirikova, Nazarov, Munkhbaatar, Munkhbayar & Terbish, 2017) occur in China? Species delimitation and identification with DNA barcoding and morphometric analyses

The *Eremias multiocellata-przewalskii* species complex is a viviparous group in the genus *Eremias*, and a well-known representative of taxonomically complicated taxa. Within this complex, a new species – *E. dzungarica* (Orlova et al., 2017) – has been described recently from western Mongolia and eastern Kazakhstan, with an apparent distribution gap in northwestern China. In this study, we used an integrative taxonomic framework to address whether *E. dzungarica* indeed occurs in China. Thirty specimens previously classified as *E. multiocellata* were collected in eastern Kazakhstan and the adjacent Altay region in China. The cytochrome *c* oxidase I (*COI*) barcodes were sequenced and compiled with those from Orlova et al. (2017) and analyzed with the standard and diverse barcoding techniques. We detected an absence of a barcoding gap in this complex, which indicates potential cryptic species in *Eremias* sp. 3 with high intraspecific diversity and multiple recently evolved species in Clade A. Both BIN and GMYC suggested an unrealistically large number of species (23 and 26, respectively), while ABGD, mPTP and BPP indicated a more conservative number of species (10, 12, and 15, respectively), largely concordant with the previously defined species-level lineages according to phylogenetic trees. Based on molecular phylogeny and morphological examination, all 30 individuals collected in this study were reliably identified as *E. dzungarica* – a distinct species – confirming the occurrence of this species in the Altay region, Xinjiang, China. Potentially owing to the larger sample size in this study, our morphological analyses revealed many inconsistencies with the original descriptions of *E. dzungarica*, which were primarily associated with sexual dimorphism and a broader range of values for various traits.

The rapid development of DNA barcoding (Hebert et al., 2003) has facilitated the successful application of a standardized short mitochondrial gene fragment, *COI*, to most species level identifications (e.g., excluding plants), species discovery and global biodiversity assessment (DeSalle & Goldstein, 2019; Yang et al., 2020). DNA barcoding is particularly helpful for phylogenetic and taxonomic inference in species groups that have considerable morphological conservatism or ambiguity (e.g., Hofmann et al., 2019; Oba et al., 2015; Xu et al., 2020; Zhang et al., 2018).

Traditional taxonomy is mainly based on morphological characters, and hence can easily lead to misidentification as a result of phenotypic plasticity, cryptic species or different morphologies at different life history stages (Bickford et al., 2007; Lee, 2004; Rock et al., 2008). Taxonomy relying on DNA barcodes alone is also unrealistic, as mitochondrial genes have many inherent biases and limitations in species delimitation, e.g., those associated with maternal inheritance, reduced population size, inconsistent mutation rate, or evolutionary processes such as purifying selection (Blair & Bryson, 2017; Pino-Bodas et al., 2013; Rubinoff et al., 2006). With the advance of barcoding techniques, however, the evidence inferred from DNA barcoding can guide further targeted morphological analysis, and the use of multiple lines of evidence, such as nuclear loci, geographical and ecological data to make more robust inferences about the species boundaries under the rubric of integrative taxonomy (Damm et

Received: 01 November 2020; Accepted: 06 April 2021; Online: 07 April 2021

Foundation items: This work was supported by the Strategic Priority Research Program of the Chinese Academy of Sciences (XDA20050201) and National Natural Science Foundation of China (32070433 to X.G.G. and 32000288 to J.L.L.)

al., 2010; Dayrat, 2005; Miller, 2007; Padial et al., 2010; Will et al., 2005).

The *Eremias multiocellata-przewalskii* species complex comprises a natural group of viviparous species in the genus *Eremias* (Guo et al., 2011; Orlova et al., 2017). The taxonomy of this species complex has been historically confusing due to the vast phenotypic variation within and among species, as well as the conservation of morphological characters in closely related species (Eremchenko et al., 1992; Eremchenko & Panfilov, 1999). So far, as many as 18 species/subspecies have been proposed across its wide distribution range covering Kyrgyzstan, eastern Kazakhstan, northern China, Mongolia, and southern Tuva Republic of Russia (Orlova et al., 2017; and references therein). Among these species is the newly delimited Dzungarian racerunner, *Eremias dzungarica* (Orlova et al., 2017). In addition to the apparent molecular and morphological deviations from congeners as described in Orlova et al. (2017), this species is characterized by a habitat preference for rocky hills and gravel ravines (“rocky form" coined in Orlova et al. (2017)) in western Mongolia at high elevations (2 400−2 600 m above sea level (a.s.l.)). However, it can also penetrate into low-altitude sandy dune areas in eastern Kazakhstan (400−1 000 m a.s.l.). As such, it remains unclear as to whether *E. dzungarica* occurs in the vast territories of the northern Junggar Depression in Xinjiang, China, between western Mongolia and eastern Kazakhstan. To date, four occurrences of so-called *E. multiocellata* (the multio-cellated racerunner) have been recorded from only two regions in the northern Junggar Depression: one in the Tacheng region and three in the Altay region reported in Zhao (1999) and Tao et al. (2018), respectively. As suggested by Orlova et al. (2017), *E. dzungarica* may have been considered as *E. multiocellata* in China, hence it is possible that these reported populations are in fact *E. dzungarica*, despite the lack of morphological and molecular data.

Orlova et al. (2017) for the first time utilized the DNA barcoding sequences (*COI*) to infer phylogenetic relationships and propose putative species in the *E. multiocellata-przewalskii* species complex based on mitochondrial lineages, incomplete morphological identification characters (e.g., no voucher specimens from certain lineages) and geographic distributions. However, they did not utilize more rigorous barcoding techniques to deeply explore the distribution of genetic distance and to test species boundaries in this species complex. To determine whether *E. dzungarica* occurs in China, we sequenced the DNA barcoding *COI* fragments and performed morphological measurement of the 30 purported *E. multiocellata* individuals collected from seven locations in eastern Kazakhstan and the adjacent western Altay region, Xinjiang, China (Figure 1A; Supplementary Table S1). Subsequently, sequences of the species complex from Orlova et al. (2017) were compiled and analyzed with diverse commonly used barcoding methods to explore the intra- and interspecific genetic distance patterns and reassess the species status of the species-level lineages proposed by Orlova et al. (2017). Finally, we explicitly identified the taxonomic status of the “multi-ocellated racerunners” collected from Kazakhstan and China with molecular and morphological data. Detailed methods are available in the Supplementary Materials and Methods.

Sequences from Orlova et al. (2017) had different lengths; most of the sequences (82.3%) were 651 bp, however some were 617−619 bp with missing data located at both ends of the sequences. To accommodate the majority of these sequences, a dataset of 651 sites was generated. A total of 81 haplotypes were determined, including four for the outgroups. 235 sites were variable, and 190 were phylogeny-informative.

The general trends of Kimura 2-parameter genetic distance indicated an increment from lower to higher taxonomic levels (Supplementary Figure S1). However, the genetic distances at the species and genus level overlapped at a low frequency (Supplementary Figure S1), indicating no apparent barcoding gap between intra- and interspecific distances. Intraspecific distances ranged from 0 to 6.18% (mean ± standard deviation

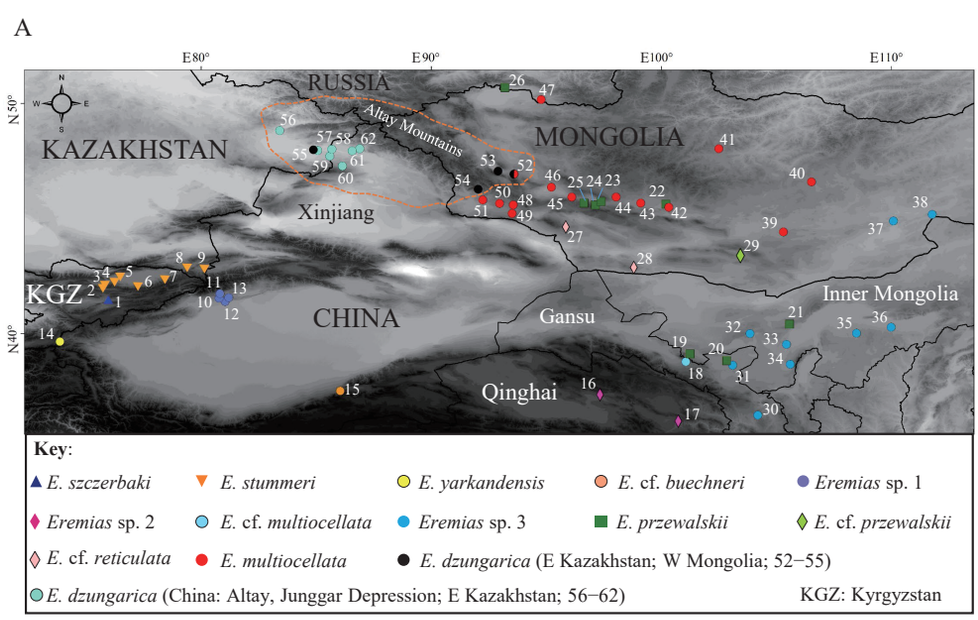

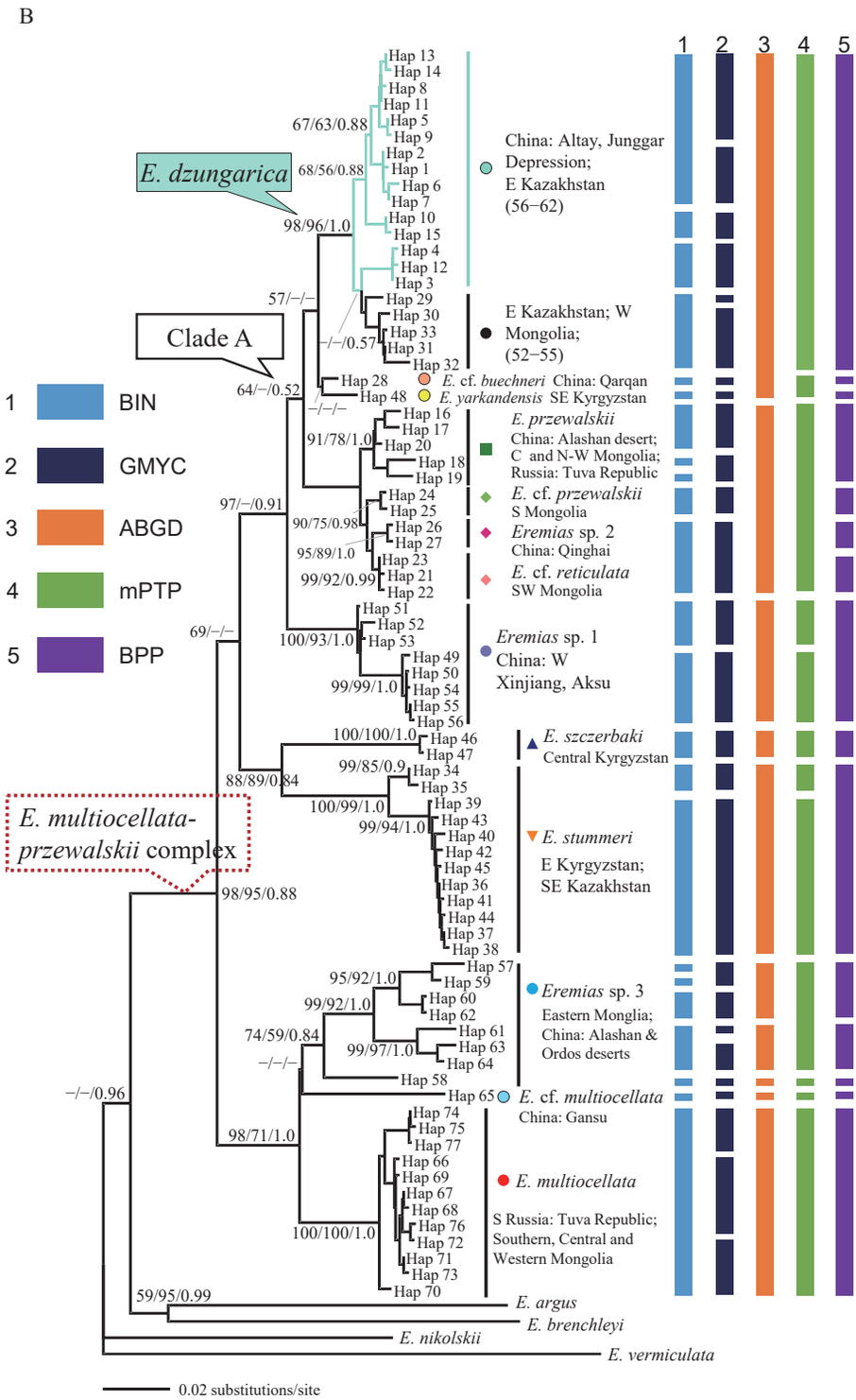

Figure 1 Collection sites of *Eremias multiocellata-przewalskii* species complex samples and phylogenetic relationships and species delimitation

A: Sites are numbered as in Supplementary Table S1. Colored symbols correspond to different lineages in Figure 1B and those in Orlova et al. (2017), except light green circles, which represent sampling sites in this study. Orange outlines distribution range of *E. dzungarica*. B: NJ tree based on barcoding mitochondrial *COI* haplotypes. Each colored vertical bar represents a species delimited by each method tested. Numbers beside the nodes indicate bootstrap support proportion (BSP) for NJ and ML as well as Bayesian posterior probabilities (BPP), respectively. Dashes beside nodes indicate support values with BSP < 50 or BPP < 0.5. Colored symbols correspond to Figure 1A, except the light green branches and light green circle, which represent the samples collected in this study.

(*SD*): 1.16% ± 0.91%, Supplementary Table S2); only *Eremias* sp. 3 exhibited variations over 3.0%, with a total frequency lower than 1.35% (Supplementary Figure S1). Interspecific divergences were highly variable (mean ± *SD*: 9.09% ± 2.54%, Supplementary Table S2), ranging from extremely low between *Eremias* sp. 2 and *E.* cf. *reticulata* (0.77%) to remarkably high between *Eremias* sp. 3 and *E. stummeri* (13.19%); only species within Clade A (Figure 1B) exhibited variations < 2.0%, with a total frequency lower than 0.62% (Supplementary Figure S1). Barcoding gap analysis indicated that the maximum intraspecific distance of each species was not always higher than the minimum distance to its nearest neighbor (Supplementary Figure S2). This evidence suggests the absence of a barcode gap. Three species (i.e., *Eremias* sp. 3, *E. przewalskii* and *E. dzungarica*) had lower distances to their nearest neighbor than their maximum intraspecific distances (Supplementary Figure S2 and Table S3). Of these, *E. dzungarica* exhibited moderately high maximum intraspecific distance (2.99%), while the interspecific distance to its nearest neighbor (*E.* cf. *buechneri*) was lower (1.87%; Supplementary Table S3).

The phylogenetic trees reconstructed with three different methods (i.e., Bayesian inference (BI), Neighbor-Joining (NJ) and Maximum Likelihood (ML)) resulted in nearly consistent topologies (Figure 1B; Supplementary Figures S3, S4), which is also congruent with that in Orlova et al. (2017). Most clades (representative of species-level lineages) were recovered with high support from all analyses, except for *Eremias* sp. 3 in which the Bayesian posterior probability was only moderate (BPP = 0.84); the bootstrap support proportions (BSP) in NJ and ML were similarly moderate as well (74 and 59, respectively). The monophyly of the *E. multiocellata-przewalskii* species complex recovered here was remarkably lower (BPP = 0.88) than in Orlova et al. (2017; BPP = 0.97), but the NJ and ML trees recovered significantly high support for monophyly (BSP = 98 and 95, respectively). More importantly, the 30 representative specimens (represented by the light green branches on the phylogenetic trees; Figure 1B and Supplementary Figures S3, S4) previously identified as *E. multiocellata* were explicitly nested within *E. dzungarica* with strong support (BPP = 1.0; BSP = 98 and 96 in NJ and ML, respectively), indicating that these taxa could be allocated to the recently described new species.

The distance (BIN)- and tree (GMYC)-based methods both suggested an unrealistically large number of putative species. The application of BIN in our barcoding dataset identified 23 operational taxonomic units (OTUs), of which only six were taxonomically concordant with previously defined species-level lineages in the BI/NJ/ML gene trees (Figure 1B). The single-threshold GMYC model indicated a multiple species scenario with strong statistical support ($p < 0.047$). The GMYC analysis results – which identified as many as 26 entities – were largely incongruent with the BI/NJ/ML gene trees regarding the number of species-level lineages (Figure 1B). However, consistent with the results of genetic distance analysis based on predefined species, no apparent barcoding gap was detected in ABGD analysis based on pairwise comparisons of sequences across the dataset (Supplementary Figure S5A). ABGD has been suggested to be a powerful tool to partition the barcoding datasets into putative species, even when intra- and interspecific genetic distances overlap (Puillandre et al., 2012). Our results support this perspective, as ABGD conservatively delimited 10 putative species in the initial and recursive partitions (i.e., 10 initial and 10−12 recursive partitions with prior intraspecific divergences, which varied from 0.1% to 0.93%; Supplementary Figure S5B), half of which were taxonomically concordant (Figure 1B). BPP analyses suggested 14 or 15 species with relatively low (BPP = 0.238) and high (BPP = 0.735) support, respectively. Within the 15 genetic clusters, four (i.e., *Eremias* sp. 2, *E.* cf. *reticulata*, *E.* cf. *buechneri* and *E. yarkandensis*) were delimited with relatively high support (BPP > 0.86 and < 0.9) and others with even stronger support (BPP > 0.95), while *E.* cf. *buechneri* and *E. yarkandensis* may form one putative species with extremely low support (BPP = 0.13). These 15 delimited genetic clusters were largely consistent with the species-level lineages in the BI/NJ/ML gene trees, except that *Eremias* sp. 3 was delimited into three genetic clusters, consistent with the results in the ABGD analysis (Figure 1B). The mPTP model exhibited relatively conservative species delimitation for our dataset with highly uneven sampling. Twelve putative species were suggested by the mPTP, but only four of them were consistent with the species-level lineages in the BI/NJ/ML gene trees (Figure 1B). Both the ABGD and BPP indicated three consistent cryptic species, and the mPTP suggested two putative species in *Eremias* sp. 3, whereas both the BIN and GMYC split this species into as many as five different genetic structures. One singleton cryptic species (Hap 58) from population 36 in eastern Inner Mongolia (Figure 1A; Supplementary Table S1) was recognized in all analyses, indicating that its taxonomic status deserves particular attention in future studies with more robust data. Moreover, the cryptic diversity in *Eremias* sp. 3 was also supported with high intraspecific pairwise divergence (3.49%−6.18%) and large morphological variations that may have been overlooked by Orlova et al. (2017) according to our field observations in Inner Mongolia.

Despite the low interspecific pairwise genetic distances (< 2%) among the lineages in Clade A (including seven species-level lineages in the BI/NJ/ML gene trees; Figure 1B), Orlova et al. (2017) considered these as distinct species for the following reasons. First, these lineages in Clade A were apparently morphologically differentiated (except *E. przewalskii* and *E.* cf. *przewalskii*). Second, these lineages covered separate geographic distributions. Similarly, our BPP analysis also suggests that all lineages in Clade A are putative species, partially supported by the BIN and GMYC analyses that congruently suggest the species status for *E.* cf. *buechneri*, *E. yarkandensis* and *E.* cf. *przewalskii* (Figure 1B). Therefore, we propose that the divergence among the lineages in Clade A is indicative of multiple recent speciation events. However, Orlova et al. (2017) did not propose any interpretation for the controversial status of *E.* cf. *przewalskii*, which morphologically resembles *E. przewalskii*, although in our study *E.* cf. *przewalskii* was not nested within *E. przewalskii* and did not form a sister taxon to *E. przewalskii* in the phylogenetic trees (Figure 1B). There are two possible explanations for this discrepancy. Firstly, *E.* cf. *przewalskii*

may be a cryptic species that has evolved morphological traits similar to *E. przewalskii*. Alternatively, *E.* cf. *przewalskii* may in fact be *E. przewalskii*, and the mitochondria of this population (site 29) had been replaced by an unknown species from the *E. multiocellata-przewalskii* species complex. With current data, however, we cannot rule out either of these hypotheses. As such, more thorough fieldwork and rigorous morphometric analyses and additional molecular data (e.g., nuclear loci) are needed for future taxonomic and evolutionary hypothesis testing for this species group.

The status of *E. dzungarica* is the most contradictory in our species delimitation analyses. Although BPP and mPTP explicitly suggested its species status, BIN and GMYC split it into many different genetic clusters while ABGD merged it with *E.* cf. *buechneri* and *E. yarkandensis* as a single putative species. Given that the monophyly of most genetic clusters in *E. dzungarica* delimited by BIN and GMYC was not strongly supported (BSP < 70; BPP < 0.9), the intraspecific differentiation in *E. dzungarica* (relatively high; maximum intraspecific divergence of 2.99%) may not have been high enough to form an independent evolutionary lineage. On the other hand, the relationships among *E. dzungarica*, *E.* cf. *buechneri* and *E. yarkandensis* were not resolved in the BI and ML trees (Supplementary Figures S3, S4). Thus, the ABGD results may be affected by the reciprocally nearest species among them (Supplementary Table S3). In addition, the BIN, GMYC and BPP analyses consistently suggested *E.* cf. *buechneri* and *E. yarkandensis* as independent species (Figure 1B); these results, in turn, suggest that *E. dzungarica* should be allocated as a distinct species. Finally, the morphological concordance among the populations of *E. dzungarica* lends further support for its distinct species status.

The range of values for most metric and meristic traits of the specimens from this study was largely consistent with that of the *E. dzungarica* individuals in Orlova et al. (2017). The only exception was the metric trait Dist.P.fm, with a larger range of values found in our study (3.52−6.34 mm) than that reported in Orlova et al. (2017) (1.60−2.50 mm; Supplementary Tables S4.1, S4.2). Moreover, statistical tests indicated that the specimens in this study were significantly different than those in Orlova et al. (2017) in four traits (Lab.total.R, Ventr., Lam.subdig. and P.fm.L; Supplementary Table S5). However, the individuals in this study can further be morphologically identified as *E. dzungarica* based on the following combination of characters: single frontonasal; two prefrontals; subocular shield not in contact with mouth margin, in touch with 6th−8th supralabials; 3−5 subocular shields; three pairs of nasals; subnasal not in contact with rostral shield, located above 1st to 3rd supralabials; two loreal shields, except one individual from Kazakhstan (Voucher No. KZL98; Supplementary Table S1) with single loreal at either side of head; 5−6 submaxillary shields at right or left side; first three pairs of submaxillary shields in contact with each other, no or minor split between last contacting pair of submaxillary shields; last submaxillary shield in contact with infralabials in certain individuals (26.7%); supraoculars separated completely from supraciliary shields by single row of granular scales in some individuals (60%), but partly in contact with supraciliary in other individuals due to deficiency of certain granular scales in the row; supraoculars in contact with frontal and frontoparietals without granular scales between them; 3−4 scales from distal femoral pore to knee; one or two explicitly enlarged shields in precloacal (preanal) area; background of dorsum and head dorsal surface grayish-brown; head dorsal surface with many (usually in males) or few (usually in females) random irregular black blotches; black blotches on ventral flanks forming two regular longitudinal rows, ventral sides near black blotch rows with sparse yellowish spots in some individuals (usually males) (Figure 2).

It should be noted that there are also some inconstancies between the morphological descriptions reported here and the original descriptions of *E. dzungarica* in Orlova et al. (2017). One of the most important findings in this study is that the sexual dimorphism related to the dorsal coloration pattern reported in Orlova et al. (2017) may be unreliable. Males are distinguished by a bright green-yellowish coloration at the third row of ocelli, while not all females lack their bright color at the third row of ocelli, and many individuals even show the same well-developed ocelli with bright color as males (Figure 2A1, A2, A4). In fact, based on our field observations, we suspect that these dorsolateral ocelli coloration patterns may be related to age, for the following reasons. Firstly, both males and females displayed the bright ocelli before adulthood. Secondly, males may retain and develop the bright ocelli to attract females for mating, while females may gradually lose them since the bright ocelli may have no benefits for them. Thirdly, losing the bright color in adult females may help them avoid predators. Lastly, for the specimens examined in this study, all males had two apparent rows of whitish ocelli near the mid-dorsum (Figure 2B1−B3), while the whitish ocelli in the first row near the mid-dorsum was blurry in some females (Figure 2A1−A3). Taken together, these phenomena may indicate another unreliable sexually dimorphic trait related to the dorsal patterning in *E. dzungarica*.

Our morphometric analyses, however, showed apparent sexual dimorphism in body size, with males usually larger than females (Supplementary Tables S4.1, S4.2). Although one metric trait (Dist.P.fm) was not sexually dimorphic, it was closely related to the number of scales between two femoral pore series (scal.f.p) instead of body size. While the values of Dist.P.fm measured in Orlova et al. (2017) were substantially lower than those in this study, there is no explicit evidence to explain why such significant deviations occur. Moreover, Orlova et al. (2017) did not report sexual dimorphism in any of the meristic traits of *E. dzungarica*, whereas we found a single meristic trait (Sq.c.cd) with significant sexual dimorphism. We also observed other inconsistencies in one individual (Voucher No. KZL98, Supplementary Table S1) from population 56 in Kazakhstan (Figure 1A; Supplementary Table S1) with a single loreal shield on both sides of the head and a broader range of values for many different traits (Supplementary Tables S4.1−S4.3). In general, these findings could be attributed to individual variation, like the fusion of two loreal shields into one, and/or to the larger sample size in this study than that in Orlova et al. (2017).

Our sampling sites in China are located in the western Altay region in Xinjiang, which is close to the known occurrences of *E. dzungarica* in eastern Kazakhstan (Orlova et al., 2017).

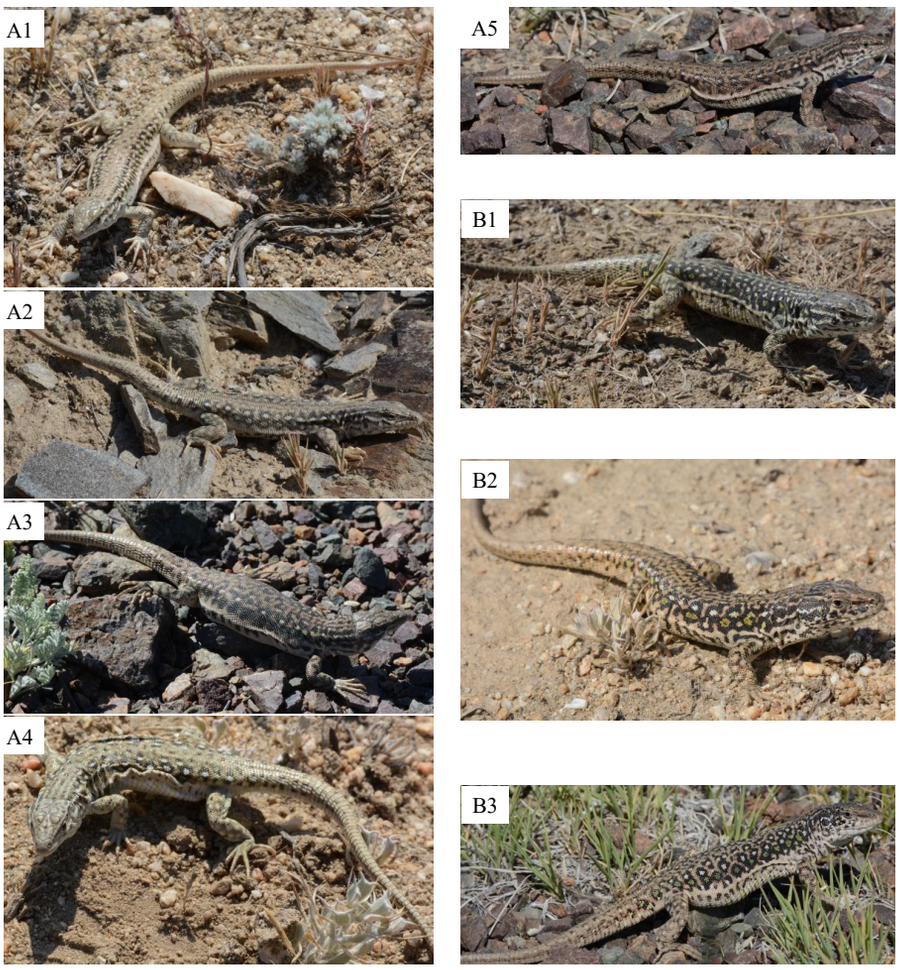

Figure 2 General view of wild specimens from field recordings in eastern Kazakhstan and western Altay region, China
A1−A5: females; B1−B3: males.

There is still a large degree of uncertainty about the existence of this species between the western Altay region and the known occurrences of *E. dzungarica* in western Mongolia near the Altay Mountains (Figure 1A). For example, Tao et al. (2018) reported three occurrences of *E. multiocellata* in the Altay region, one located in the west, close to our sampling localities, and two in the central and eastern parts. Although the precise taxonomic assignment of these populations is unknown, we suspect they could be allocated to *E. dzungarica*, given that this species may have a continuous distribution range from eastern Kazakhstan to western Mongolia. The habitats of *E. dzungarica* are described in Orlova et al. (2017) as rocky hills and ravines at elevations up to 2 400−2 600 m a.s.l. in Mongolia, and sandy dunes (400−600 m a.s.l.) and occasional rocky outcrops (1 000 m a.s.l.) at lower elevations in Kazakhstan. Consistent with these habitat descriptions, the populations from Kazakhstan sampled here were also associated with sandy dunes (~400 m a.s.l.). The habitats of individuals sampled from the western Altay region in China were more diverse, and included sandy dunes (sites 58, 59 and 61; 420−580 m a.s.l.; Figure 1A) at similar elevations, rocky outcrops (site 62; ~620 m a.s.l.), and rocky ravines (site 60; ~1 200 m a.s.l.; Figure 1A) at higher elevations. Considering that *E. dzungarica* can inhabit a wide range of altitudes, future fieldwork on this species should be conducted in the vast low-elevation territories from eastern Kazakhstan to western Mongolia, as well as the high-elevation territories in the Altay Mountain areas that span all three countries.

SCIENTIFIC FIELD SURVEY PERMISSION INFORMATION

Permission for field surveys was granted by the Forestry Department and National Reserves of China and Committee for Forestry and Hunting of the Ministry of Environmental Protection of Kazakhstan.

SUPPLEMENTARY DATA

Supplementary data to this article can be found online.

COMPETING INTERESTS

The authors declare that they have no competing interests.

AUTHORS' CONTRIBUTIONS

X.G.G and J.L.L. designed the study. J.L.L., T.N.D., M.A.C.,

X.G., and D.J.L. collected specimens in the field. J.L.L., X.G., and D.J.L. performed molecular experiments. J.L.L. and M.A.C. measured the specimens. J.L.L. performed data analyses. J.L.L., X.G.G and T.N.D. wrote and revised the manuscript. All authors read and approved the final version of the manuscript.

ACKNOWLEDGEMENTS

We thank three anonymous referees for insightful comments and Dr. Jacquelin DeFaveri for language editing.

Jin-Long Liu[1], Tatjana N. Dujsebayeva[2], Marina A. Chirikova[2], Xiong Gong[1], Da-Jiang Li[1], Xian-Guang Guo[1,*]

[1] *Chengdu Institute of Biology*, *Chinese Academy of Sciences*, *Chengdu* 610041, *China*

[2] *Institute of Zoology of Republic of Kazakhstan*, *Almaty* 050060, *Kazakhstan*

*Corresponding author, E-mail: guoxg@cib.ac.cn

REFERENCES

Bickford D, Lohman DJ, Sodhi NS, Ng PKL, Meier R, Winker K, et al. 2007. Cryptic species as a window on diversity and conservation. *Trends in Ecology & Evolution*, **22**(3): 148−155.

Blair C, Bryson Jr RW. 2017. Cryptic diversity and discordance in single-locus species delimitation methods within horned lizards (Phrynosomatidae: *Phrynosoma*). *Molecular Ecology Resources*, **17**(6): 1168−1182.

Damm S, Schierwater B, Hadrys H. 2010. An integrative approach to species discovery in odonates: from character-based DNA barcoding to ecology. *Molecular Ecology*, **19**(18): 3881−3893.

Dayrat B. 2005. Towards integrative taxonomy. *Biological Journal of the Linnean Society*, **85**(3): 407−417.

DeSalle R, Goldstein P. 2019. Review and interpretation of trends in DNA barcoding. *Frontiers in Ecology and Evolution*, **7**: 302.

Eremchenko VK, Panfilov AM. 1999. Taxonomic situation of multiocellated racerunner of the "multiocellata" - complex of Kyrghyzstan and neighbor China (Sauria: Lacertidae: *Eremias*). *Science and New Technologies*, **4**: 112−124.

Eremchenko VK, Panfilov AM, Tzarinenko EI. 1992. *Eremias multiocellata* complex: solution of some problems in systematics of the multiocellated racerunners of Kyrgyzstan (Sauria, Lacertidae, *Eremias*). *In*: Conspectus of the Researches on Cytogenetics and Systematics of Some Asiatic Species of Scincidae and Lacertidae. Ilim, Bishkek, 65-80. (in Russian)

Guo XG, Dai X, Chen DL, Papenfuss TJ, Ananjeva NB, Melnikov DA, et al. 2011. Phylogeny and divergence times of some racerunner lizards (Lacertidae: *Eremias*) inferred from mitochondrial 16S rRNA gene segments. *Molecular Phylogenetics and Evolution*, **61**(2): 400−412.

Hebert PDN, Ratnasingham S, deWaard JR. 2003. Barcoding animal life: cytochrome c oxidase subunit 1 divergences among closely related species. *Proceedings of the Royal Society B: Biological Sciences*, **270**(Suppl 1): S96−S99.

Hofmann EP, Nicholson KE, Luque-Montes IR, Köhler G, Cerrato-Mendoza CA, Medina-Flores M, et al. 2019. Cryptic diversity, but to what extent? Discordance between single-locus species delimitation methods within mainland anoles (Squamata: Dactyloidae) of northern central America. *Frontiers in Genetics*, **10**: 11.

Lee MSY. 2004. The molecularisation of taxonomy. *Invertebrate Systematics*, **18**(1): 1−6.

Miller SE. 2007. DNA barcoding and the renaissance of taxonomy. *Proceedings of the National Academy of Sciences of the United States of America*, **104**(12): 4775−4776.

Oba Y, Ôhira H, Murase Y, Moriyama A, Kumazawa Y. 2015. DNA barcoding of Japanese click beetles (Coleoptera, Elateridae). *PLoS One*, **10**(1): e0116612.

Orlova VF, Poyarkov Jr NA, Chirikova MA, Nazarov RA, Munkhbaatar M, Munkhbayar K, et al. 2017. MtDNA differentiation and taxonomy of Central Asian racerunners of Eremias multiocellata-E. *przewalskii species complex (Squamata, Lacertidae)*. *Zootaxa*, **4282**(1): 1−42.

Padial JM, Miralles A, De la Riva I, Vences M. 2010. The integrative future of taxonomy. *Frontiers in Zoology*, **7**(1): 16.

Pino-Bodas R, Martín MP, Burgaz AR, Lumbsch HT. 2013. Species delimitation in *Cladonia* (Ascomycota): a challenge to the DNA barcoding philosophy. *Molecular Ecology Resources*, **13**(6): 1058−1068.

Puillandre N, Lambert A, Brouillet S, Achaz G. 2012. ABGD, Automatic Barcode Gap Discovery for primary species delimitation. *Molecular Ecology*, **21**(8): 1864−1877.

Rock J, Costa FO, Walker DI, North AW, Hutchinson WF, Carvalho GR. 2008. DNA barcodes of fish of the Scotia Sea, Antarctica indicate priority groups for taxonomic and systematics focus. *Antarctic Science*, **20**(3): 253−262.

Rubinoff D, Cameron S, Will K. 2006. A genomic perspective on the shortcomings of mitochondrial DNA for "barcoding" identification. *Journal of Heredity*, **97**(6): 581−594.

Tao XQ, Cui SP, Jiang ZG, Chu HJ, Li N, Yang DD, et al. 2018. Reptilian fauna and elevational patterns of the reptile species diversity in Altay Prefecture in Xinjiang, China. *Biodiversity Science*, **26**(6): 578−589. (in Chinese)

Will KW, Mishler BD, Wheeler QD. 2005. The perils of DNA barcoding and the need for integrative taxonomy. *Systematic Biology*, **54**(5): 844−851.

Xu X, Kuntner M, Bond JE, Ono H, Ho SYW, Liu FX, et al. 2020. Molecular species delimitation in the primitively segmented spider genus *Heptathela* endemic to Japanese islands. *Molecular Phylogenetics and Evolution*, **151**: 106900.

Yang CQ, Lv Q, Zhang AB. 2020. Sixteen years of DNA barcoding in China: What has been done? What can be done?. *Frontiers in Ecology and Evolution*, **8**: 57.

Zhang F, Jantarit S, Nilsai A, Stevens MI, Ding YH, Satasook C. 2018. Species delimitation in the morphologically conserved *Coecobrya* (Collembola: Entomobryidae): a case study integrating morphology and molecular traits to advance current taxonomy. *Zoologica Scripta*, **47**(3): 342−356.

Zhao KT. 1999. Lacertidae. *In*: Zhao EM, Zhao KT, Zhou KY. Fauna Sinica, Reptilia (Squamata: Lacertilia), Vol. 2. Beijing: Science Press, 231–236. (in Chinese)

Supplementary Materials

Supplementary Materials and Methods

Sampling

During 2014 and 2017, we conducted a joint Sino-Kazh field investigation on the herpetofauna in eastern Kazakhstan and the adjacent Junggar Depression in China. Thirty specimens (15 males, 15 females) from seven sites were collected from eastern Kazakhstan and northwestern Altay region, Xinjiang, China (Supplementary Figure S1 and Table S1), which were initially identified as *E. multiocellata*. The lizards were euthanized with an overdose of sodium pentobarbital via intraperitoneal injection, and liver or tail tissues were extracted and preserved in 95% ethanol following the animal use protocols approved by the Chengdu Institute of Biology (CIB), Chinese Academy of Sciences (CAS). All voucher specimens are preserved in CIB, CAS.

Molecular data collection

Genomic DNA was extracted from liver or tail tissues following the modified high-salt protocol proposed by Aljanabi & Martinez (1997). Fragments of the mitochondrial *COI* gene (709 bp) were amplified via polymerase chain reaction (PCR) using primers designed according to Ward et al. (2005) with minor modifications (E_COIF 5'-TCAACCAACCACAAAGACATTGGCAC-3' and E_COIR 5'-TAGACTTCTGGGTGGCCAAAGAATCA-3'). The PCR reaction mixture contained 12.5 μL of 2 × EasyTaq SuperMix (Tsingke Biol-Tech, Chengdu, China), 0.2 μM of each primer, and 1–2 μL of genomic DNA for a total volume of 25 μL. The amplification protocols included an initial denaturation at 94 °C for 4 min, followed by 35 cycles of 94 °C for 30 s, 52 °C for 30 s and elongation at 72 °C for 50 s, and a final extension at 72 °C for 10 min. All PCR products were commercially purified and sequenced for double strands with the primers used for amplification. All novel sequences were deposited in GenBank under the accession numbers MW172523−MW172552.

Nineteen individuals from China and 11 from Kazakhstan were sequenced for *COI*. All novel sequences were translated to amino acids with MEGA v7.0.26 (Kumar et al., 2016), and no stop codons were detected. In total, 156 sequences – which included those from Orlova et al. (2017) (available in GenBank) – were aligned using Clustal X v2.0 (Larkin et al., 2007) with default settings. Identical sequences were collapsed into a single haplotype using DnaSP v5.0 (Librado & Rozas, 2009).

DNA barcoding diversity analysis

The dataset containing all sequences was uploaded into the BOLD system under the project '*Eremias multiocellata-przewalskii* complex barcoding' (Barcode of Life Data System website, www.barcodinglife.com; Ratnasingham & Hebert, 2007). We measured the genetic distance with the Kimura 2-parameter (K2P; Kimura, 1980) model, which has been widely used in barcoding studies. The intraspecific and intra-genus pairwise distances were calculated with the 'Distance Summary' analysis tool in BOLD. The maximum intraspecific genetic distance and corresponding minimum distance to nearest neighbor at the species level were calculated and compared using the 'Barcoding Gap Analysis' tool in BOLD.

Phylogenetic analysis

The neighbor-joining (NJ) (Saitou & Nei, 1987) tree was constructed in MEGA with a gamma distribution rate variation among sites (shape parameter = 4) and pairwise deletion option for the treatment of missing data. Bootstrap support for clades was evaluated by nonparametric bootstrap analysis (Felsenstein, 1985) with 1 000 replicates. Bayesian inference (BI) was conducted with MrBayes v3.2.2 (Ronquist et al., 2012). The best-fit models of nucleotide substitution for each partition scheme were selected using PartitionFinder v2.1.1 (Lanfear et al., 2017). Three codon partitions and their corresponding substitution model for the *COI* gene sequences were proposed: first codon, K80+G+I; second codon, F81; third codon, GTR+G. Two parallel runs of one cold and three heated Monte Carlo Markov chains (MCMCs) were performed with sampling every 200 generations and were automatically stopped

after reaching a mean standard deviation between split frequencies of less than 0.01. Parameters and topologies were estimated from 13 405 steps after discarding the first 30%. Convergence of the runs was assessed by effective sample size (ESS ≥ 200) with Tracer v1.7.1 (Rambaut et al., 2018). Partitioned ML (Maximum Likelihood) analyses were conducted in RAxML v8.2.4 (Stamatakis, 2014) with the GTR+G model for all subsets. A complete random starting tree (option -d) was initiated with 100 independent search replicates where the tree with the best likelihood was chosen. Bootstrap support proportion (BSP) for the clades was obtained with a sufficient number of bootstrap replicates (450), which was automatically determined by setting the default cutoff threshold (option -# autoMRE).

Species delimitation

We first employed two distance-based methods dedicated to barcoding datasets. The Barcode Index Number (BIN) system clusters (Ratnasingham & Hebert, 2013) was conducted with the 'BIN Discordance' option in BOLD, which was employed to assign individuals to operational taxonomic units (OTUs) that represent presumable species. The BIN system uses the refined single linkage algorithm (RESL) for clustering process, and hence is independent of any prior taxonomic assignment. Similarly, Automatic Barcode Gap Discovery (ABGD; Puillandre et al., 2012) does not need *a priori* species hypotheses, and clusters sequences into candidate species by detecting a 'barcode gap' that demarcates intra- and interspecific distance. Analysis was implemented in the ABGD web server (https://bioinfo.mnhn.fr/abi/public/abgd/abgdweb.html) with the K2P model and other parameters as default.

Two coalescent methods were further employed to delimit species: the generalized mixed Yule coalescent (GMYC) model implemented in the GMYC web server (http://species.h-its.org/gmyc/), and Bayesian species identification under the multispecies coalescent (MSC) model with the program BPP v3.3 (Yang & Rannala, 2010). GMYC was proposed to delimit species using the reconstructed gene tree for a single locus (Fujisawa & Barraclough, 2013). We reconstructed ultrametric gene trees

in BEAST v1.8.2 (Drummond et al., 2012) with three codon partitions. The substitution models were calculated in PartitionFinder; the first codon used K80+G+I, the second used HKY, and the third used TRN+G. To reduce compounding errors from time calibration uncertainties or molecular substitution rates, we left the prior 'clock.rate' to default 1.0. Posterior samplings were drawn every 1 000 steps over 15 million MCMC steps with the uncorrelated lognormal relaxed clock model and Yule speciation tree prior. Two independent runs were performed. Stationarity of the Markov chains for each run was checked using Tracer for ESS ≥ 200. Finally, the tree files were combined using LogCombiner v1.8.2, and a maximum clade credibility (MCC) tree with median node heights was generated with TreeAnnotator after discarding the first 25% of posterior sampling as burn-in. The MCC tree was used as an input in the single-threshold GMYC analysis implemented in the GMYC server. Bayesian species identification under the MSC model was considered to have better performance in species assignment than other single-locus delimiting methods for DNA barcoding analyses (Yang & Rannala, 2017). We ran the A11 model with the presumption of relatively large ancestral population sizes (θ ~ G (1, 200)) and deep divergence (τ_0 ~ G (1.5, 10)); this single set of priors was based on our unpublished data (Liu, 2019). To explore the potential cryptic species within our study system, we designated the significantly supported lineages within *E. stummeri* (two reciprocal monophyletic lineages) and *Eremias* sp. 3 (two reciprocal monophyletic lineages and a singleton) as different unique populations in our prior population assignments in the imap file. The reversible-jump Markov chain Monte Carlo (rjMCMC) algorithm 1 with parameters combination (α, m) = (1, 0.5) and speciesmodelprior = 1 were used to repeat the BPP runs twice with different starting seeds to assess the consistency between the different runs. Each run was conducted with rjMCMC analysis for 500 000 generations (sampling interval of five), with the first 20 000 samples discarded as burn-in.

In addition, species delimitation with the multi-rate Poisson tree processes model (mPTP) has been shown to have reliable performance (Blair & Bryson, 2017), as it explicitly accounts for differences in sampling intensity and/or effective population

sizes of species (Kapli et al., 2017). We implemented mPTP analysis in the web server (https://mptp.h-its.org) using the MCC tree constructed in the previous BEAST analysis.

All species delineation analyses described above were conducted with haplotypes (except BIN, which used all sequences) and without outgroups.

Morphological analyses

Morphological measurement was performed on all 30 specimens collected in this study, following the traits analyzed in Szczerbak (1974), Dujsebayeva et al. (2009), and Orlova et al. (2017). Morphological analyses were conducted with 11 metric and 12 meristic traits (Supplementary Table S5). Of these traits, four meristic traits (Supplementary Table S5) were counted on both the left and right sides of the body. Metric measurements were conducted using a digital caliper and recorded to two decimal places.

We first employed analysis of variance (ANOVA) to test for sexual dimorphism in both metric and meristic datasets collected in this study. All metric traits (except Dist.P.fm) and one meristic trait (Sq.c.cd) exhibited significant sexual dimorphism ($p < 0.05$). As a result, the comparative demonstration of these sex-dependent characters (values given as ranges and means ± SE) between the individuals from this study and the holotype and paratypes of *E. dzungarica* from Orlova et al. (2017) were given separately for males and females. The values of the other age- and sex-independent metric and meristic characters were calculated for all specimens combined (including males, females and juveniles in this study and Orlova et al. (2017), respectively). Moreover, to test whether the specimens in this study differed significantly from *E. dzungarica* in morphological traits with a sample size greater than 11, we performed a two independent samples *t*-test. All morphometric analyses were performed with SPSS 19 (SPSS Inc., Chicago, USA).

REFERENCES

Aljanabi SM, Martinez I. 1997. Universal and rapid salt-extraction of high quality genomic DNA for PCR-based techniques. *Nucleic Acids Research*, **25**(22): 4692−4693.

Blair C, Bryson Jr RW. 2017. Cryptic diversity and discordance in single-locus species delimitation methods within horned lizards (Phrynosomatidae: *Phrynosoma*). *Molecular Ecology Resources*, **17**(6): 1168−1182.

Drummond AJ, Suchard MA, Xie D, Rambaut A. 2012. Bayesian phylogenetics with BEAUti and the BEAST 1.7. *Molecular Biology and Evolution*, **29**(8): 1969−1973.

Dujsebayeva TN, Chirikova MA, Belyalov OV. 2009. New finds of the racerunner of *Eremias multiocellata* complex in Kazakhstan. *Russian Journal of Herpetology*, **16**(1): 51−56.

Felsenstein J. 1985. Confidence limits on phylogenies: an approach using the bootstrap. *Evolution*, **39**(4): 783−791.

Fujisawa T, Barraclough TG. 2013. Delimiting species using single-locus data and the Generalized Mixed Yule Coalescent approach: a revised method and evaluation on simulated data sets. *Systematic Biology*, **62**(5): 707−724.

Kapli P, Lutteropp S, Zhang J, Kobert K, Pavlidis P, Stamatakis A, et al. 2017. Multi-rate Poisson tree processes for single-locus species delimitation under maximum likelihood and Markov chain Monte Carlo. *Bioinformatics*, **33**(11): 1630−1638.

Kimura M. 1980. A simple method for estimating evolutionary rates of base substitutions through comparative studies of nucleotide sequences. *Journal of Molecular Evolution*, **16**(2): 111–120.

Kumar S, Stecher G, Tamura K. 2016. MEGA7: molecular evolutionary genetics analysis version 7.0 for bigger datasets. *Molecular Biology and Evolution*, **33**(7): 1870−1874.

Lanfear R, Frandsen PB, Wright AM, Senfeld T, Calcott B. 2017. Partitionfinder 2:

new methods for selecting partitioned models of evolution for molecular and morphological phylogenetic analyses. *Molecular Biology and Evolution*, **34**(3): 772−773.

Larkin MA, Blackshields G, Brown NP, Chenna R, McGettigan PA, McWilliam H, et al. 2007. Clustal W and Clustal X version 2.0. *Bioinformatics*, **23**(21): 2947−2948.

Librado P, Rozas J. 2009. DnaSP v5: a software for comprehensive analysis of DNA polymorphism data. *Bioinformatics*, **25**(11): 1451−1452.

Liu J. 2019. Molecular Phylogeny and Phylogeography of *Eremias velox* Complex and *Eremias multiocellata* Complex. Ph.D. dissertation, Sichuan University, Chengdu. (in Chinese)

Orlova VF, Poyarkov Jr NA, Chirikova MA, Nazarov RA, Munkhbaatar M, Munkhbayar K, et al. 2017. MtDNA differentiation and taxonomy of Central Asian racerunners of *Eremias multiocellata-E. przewalskii* species complex (Squamata, Lacertidae). *Zootaxa*, **4282**(1): 1−42.

Puillandre N, Lambert A, Brouillet S, Achaz G. 2012. ABGD, Automatic Barcode Gap Discovery for primary species delimitation. *Molecular Ecology*, **21**(8): 1864−1877.

Rambaut A, Drummond AJ, Xie D, Baele G, Suchard MA. 2018. Posterior summarization in Bayesian phylogenetics using Tracer 1.7. *Systematic Biology*, **67**(5): 901−904.

Ratnasingham S, Hebert PDN. 2007. BOLD: The Barcode of Life Data System (http://www.barcodinglife.org). *Molecular Ecology Notes*, **7**(3): 355−364.

Ratnasingham S, Hebert PDN. 2013. A DNA-based registry for all animal species: the Barcode Index Number (BIN) system. *PLoS One*, **8**(7): e66213.

Ronquist F, Teslenko M, van der Mark P, Ayres DL, Darling A, Höhna S, et al. 2012. MrBayes 3.2: efficient Bayesian phylogenetic inference and model choice across a large model space. *Systematic Biology*, **61**(3): 539−542.

Saitou N, Nei M. 1987. The neighbor-joining method: a new method for reconstructing phylogenetic trees. *Molecular Biology and Evolution*, **4**(4):

406−425.

Stamatakis A. 2014. RAxML version 8: a tool for phylogenetic analysis and post-analysis of large phylogenies. *Bioinformatics*, **30**(9): 1312−1313.

Szczerbak NN. 1974. Yashchurki Palearktiki (*Eremias* Lizards of the Palearctic). Kiev: Naukova Dumka Press. (in Russian)

Ward RD, Zemlak TS, Innes BH, Last PR, Hebert PDN. 2005. DNA barcoding Australia's fish species. *Philosophical Transactions of the Royal Society B: Biological Sciences*, **360**(1462): 1847−1857.

Yang ZH, Rannala B. 2010. Bayesian species delimitation using multilocus sequence data. *Proceedings of the National Academy of Sciences of the United States of America*, **107**(20): 9264−9269.

Yang ZH, Rannala B. 2017. Bayesian species identification under the multispecies coalescent provides significant improvements to DNA barcoding analyses. *Molecular Ecology*, **26**(11): 3028−3036.

Figure S1

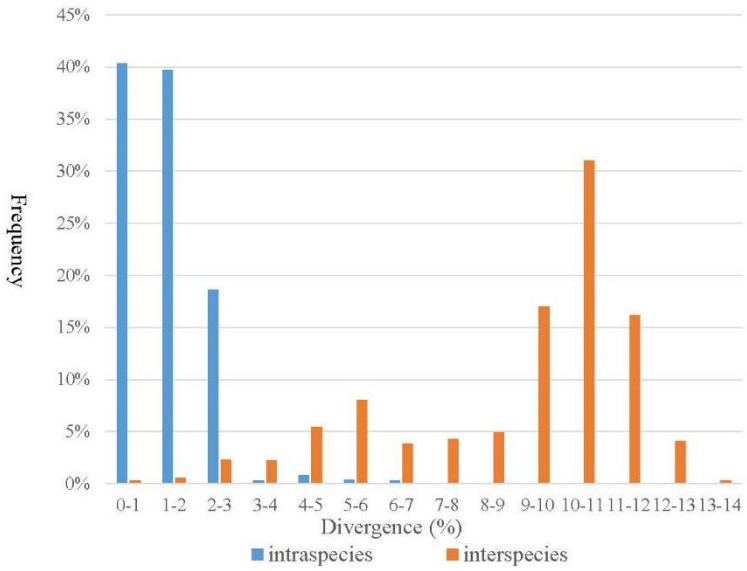

Supplementary Figure S1 Frequency distribution of pairwise Kimura 2-parameter (K2P) distances (%) at intra- and interspecific taxonomic level in *Eremias multiocellata-przewalskii* species complex

Figure S2

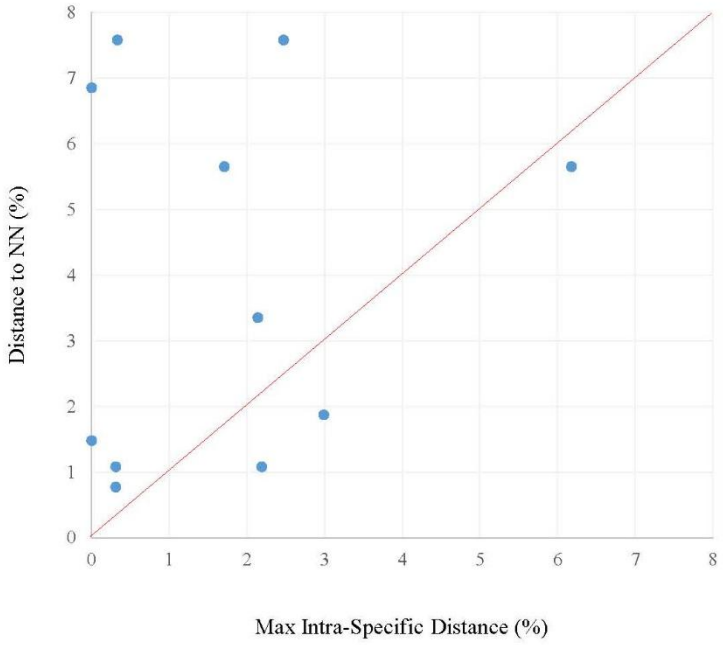

Supplementary Figure S2 Scatterplot of maximum intraspecific variation and minimum genetic distance to the nearest-neighbor species for each species in *Eremias multiocellata-przewalskii* species complex

Fig. S3

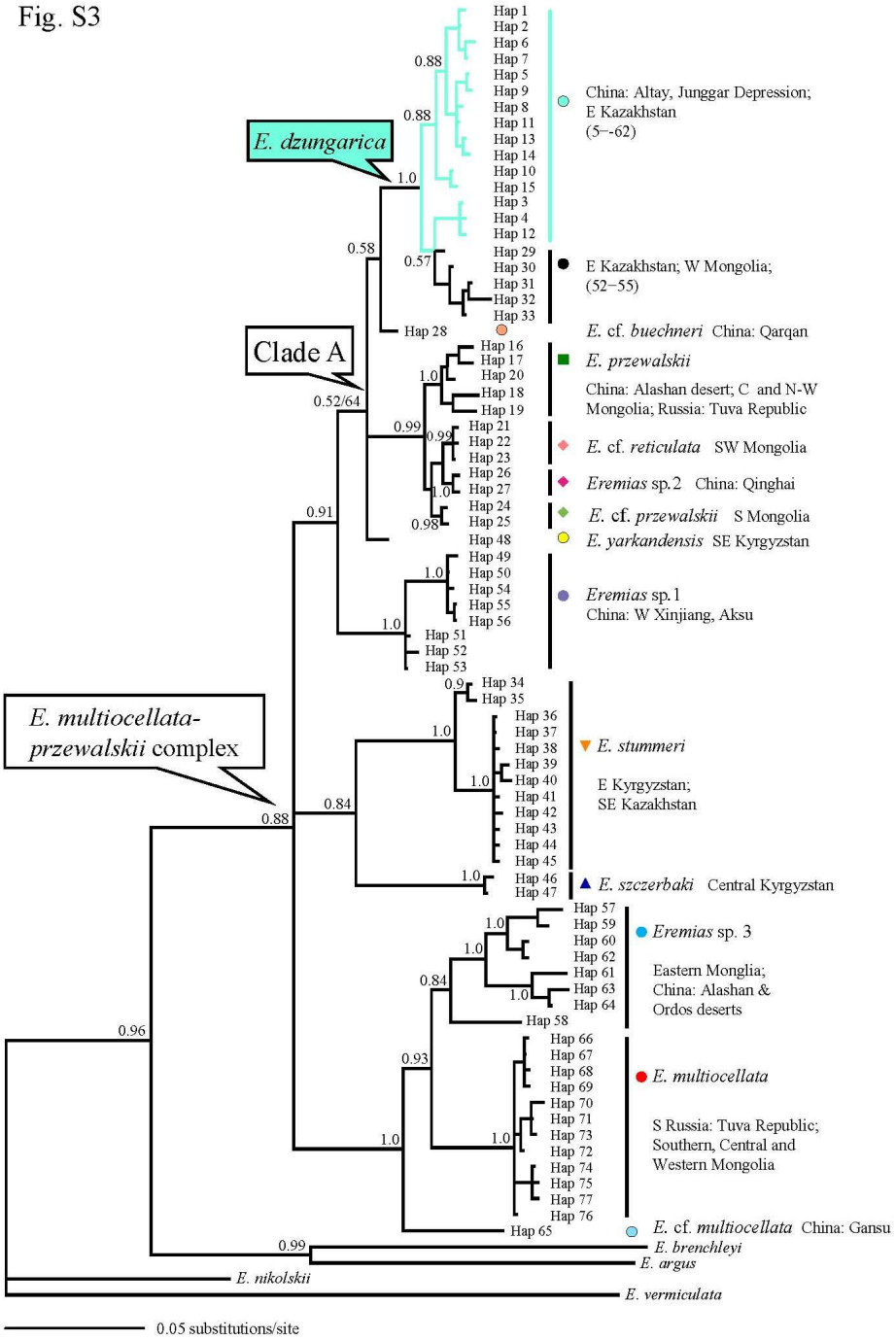

Supplementary Figure S3 50% majority-rule consensus tree of *E. multiocellata-przewalskii* species complex resulting from partitioned Bayesian analysis based on barcoding *COI* haplotypes

Numbers beside nodes indicate Bayesian posterior probabilities (BPP). Colored symbols correspond to Figure 1 and those in Orlova et al. (2017), except light green branches and light green circle, which represent samples collected in this study.

Fig. S4

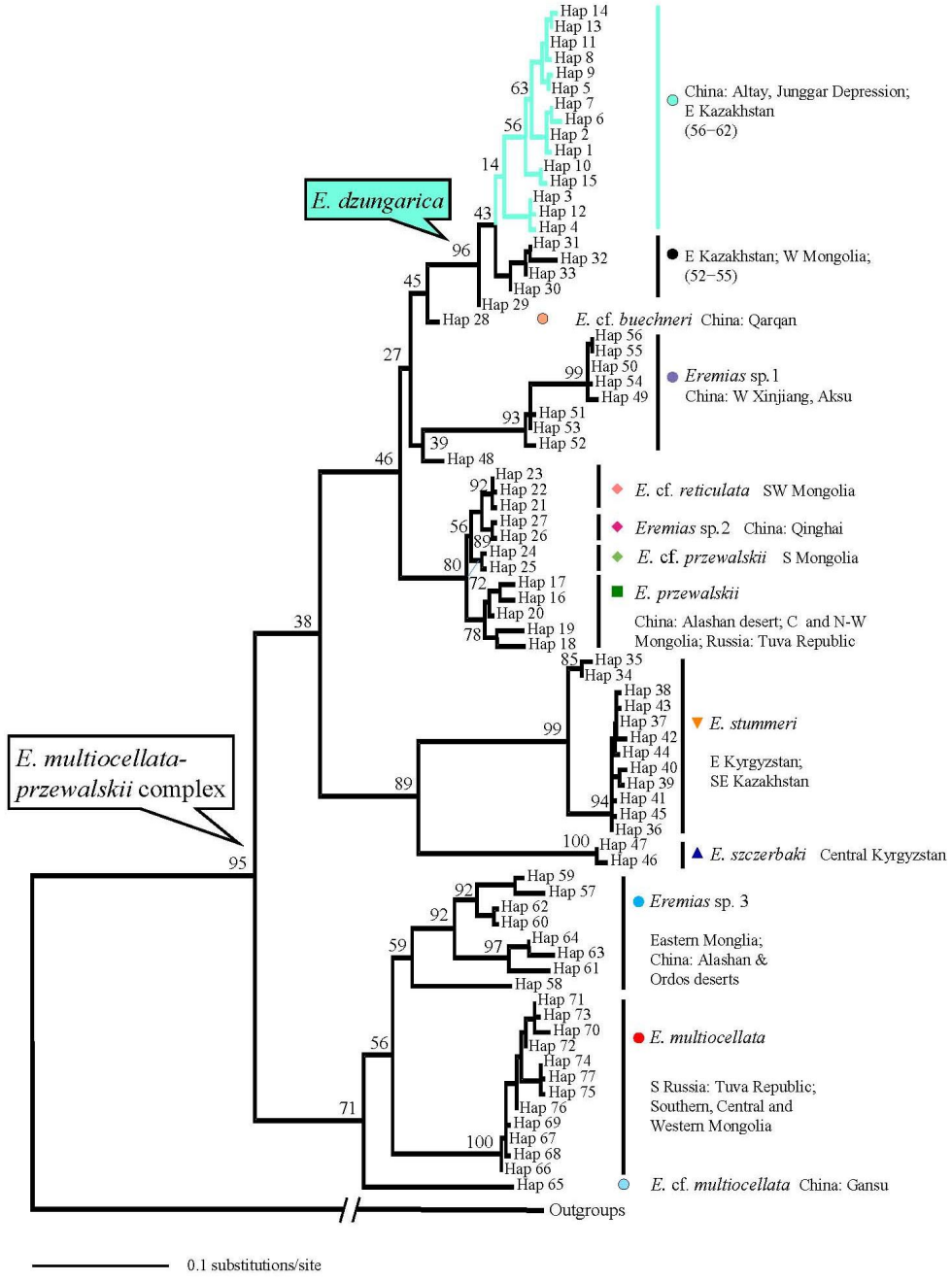

Supplementary Figure S4 Maximum-likelihood (ML) tree of *E. multiocellata-przewalskii* species complex resulting from partitioned ML analysis based on barcoding *COI* haplotypes

Numbers beside nodes indicate bootstrap support proportion (BSP). Colored symbols correspond to Figure 1 and those in Orlova et al. (2017), except light green branches and light green circle, which represent samples collected in this study.

Figure S5

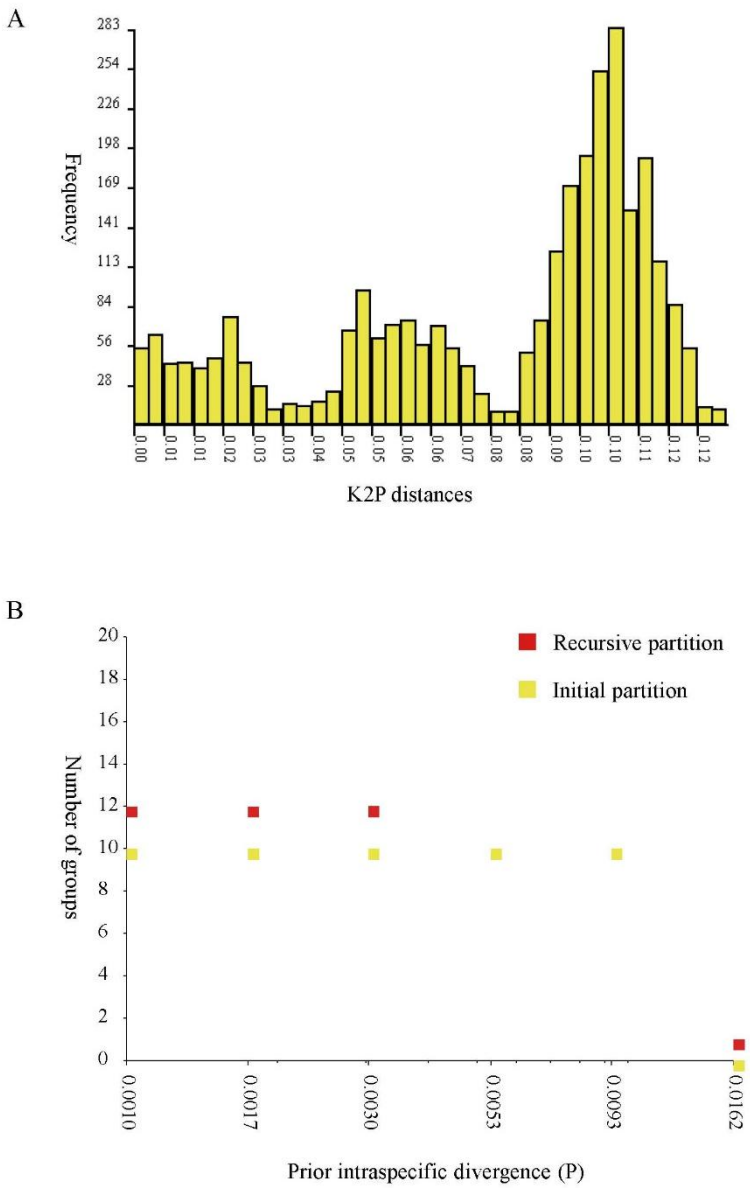

Supplementary Figure S5 Automatic Barcode Gap Discovery (ABGD) species delimitation

A: Frequency histogram of Kimura 2-parameter (K2P) pairwise distances for all barcoding mitochondrial *COI* haplotypes. B: Partitions under different prior intraspecific divergences.

Supplementary Table S1 List of analyzed specimens, along with their sex, geographic origin and GenBank accession number

Taxon	Voucher No.	Sex	Population	Haplotype No.	Locality	Longitude	Latitude	GenBank No.	Reference
E. dzungarica	KZL91	♀	56	Hap 10	near the bank of Irtysh river, Bastaushy, Kokpekti District, Kazakhstan	83.42	48.82	MW172548	This study
E. dzungarica	KZL96	♀	56	Hap 10	near the bank of Irtysh river, Bastaushy, Kokpekti District, Kazakhstan	83.42	48.82	MW172549	This study
E. dzungarica	KZL97	♂	56	Hap 10	near the bank of Irtysh river, Bastaushy, Kokpekti District, Kazakhstan	83.42	48.82	MW172550	This study
E. dzungarica	KZL98	♂	56	Hap 15	near the bank of Irtysh river, Bastaushy, Kokpekti District, Kazakhstan	83.42	48.82	MW172551	This study
E. dzungarica	KZL99	♂	56	Hap 10	near the bank of Irtysh river, Bastaushy, Kokpekti District, Kazakhstan	83.42	48.82	MW172552	This study
E. dzungarica	KZL100	♀	56	Hap 10	near the bank of Irtysh river, Bastaushy, Kokpekti District, Kazakhstan	83.42	48.82	MW172542	This study
E. dzungarica	KZL111	♀	57	Hap 11	near the bank of Irtysh river, Zaisan desert, Kazakhstan	85.08	47.95	MW172543	This study
E. dzungarica	KZL113	♀	57	Hap 12	near the bank of Irtysh river, Zaisan desert, Kazakhstan	85.08	47.95	MW172544	This study
E. dzungarica	KZL114	♀	57	Hap 3	near the bank of Irtysh river, Zaisan desert, Kazakhstan	85.08	47.95	MW172545	This study
E. dzungarica	KZL115	♀	57	Hap 13	near the bank of Irtysh river, Zaisan desert, Kazakhstan	85.08	47.95	MW172546	This study
E. dzungarica	KZL116	♂	57	Hap 14	near the bank of Irtysh river, Zaisan desert, Kazakhstan	85.08	47.95	MW172547	This study

E. dzungarica	Guo8275	♀	58	Hap 3	Western Habahe County, Xinjiang, China	85.69	48.01	MW172538	This study
E. dzungarica	Guo8276	♂	58	Hap 5	Western Habahe County, Xinjiang, China	85.69	48.01	MW172539	This study
E. dzungarica	Guo8278	♀	58	Hap 5	Western Habahe County, Xinjiang, China	85.69	48.01	MW172540	This study
E. dzungarica	Guo8279	♂	58	Hap 9	Western Habahe County, Xinjiang, China	85.69	48.01	MW172541	This study
E. dzungarica	Guo3034	♂	59	Hap 3	Zaisan desert, Jeminay County, Xinjiang, China	85.60	47.71	MW172526	This study
E. dzungarica	Guo3035	♂	59	Hap 3	Zaisan desert, Jeminay County, Xinjiang, China	85.60	47.71	MW172527	This study
E. dzungarica	Guo3036	♂	59	Hap 4	Zaisan desert, Jeminay County, Xinjiang, China	85.60	47.71	MW172528	This study
E. dzungarica	Guo3023	♂	60	Hap 1	Southeast Jeminay County, Xinjiang, China	86.15	47.28	MW172523	This study
E. dzungarica	Guo3024	♀	60	Hap 1	Southeast Jeminay County, Xinjiang, China	86.15	47.28	MW172524	This study
E. dzungarica	Guo3026	♂	60	Hap 2	Southeast Jeminay County, Xinjiang, China	86.15	47.28	MW172525	This study
E. dzungarica	Guo8240	♂	61	Hap 8	Southeast Habahe County, Xinjiang, China	86.58	47.94	MW172534	This study
E. dzungarica	Guo8241	♂	61	Hap 5	Southeast Habahe County, Xinjiang, China	86.58	47.94	MW172535	This study
E. dzungarica	Guo8242	♀	61	Hap 5	Southeast Habahe County, Xinjiang, China	86.58	47.94	MW172536	This study
E. dzungarica	Guo8243	♀	61	Hap 5	Southeast Habahe County, Xinjiang, China	86.58	47.94	MW172537	This study
E. dzungarica	Guo3096	♀	62	Hap 5	Baishashan desert, Habahe County, Xinjiang, China	86.90	48.03	MW172529	This study
E. dzungarica	Guo3097	♂	62	Hap 6	Baishashan desert, Habahe County, Xinjiang, China	86.90	48.03	MW172530	This study
E. dzungarica	Guo3098	♀	62	Hap 7	Baishashan desert, Habahe County, Xinjiang, China	86.90	48.03	MW172531	This study
E. dzungarica	Guo3099	♂	62	Hap 5	Baishashan desert, Habahe County, Xinjiang, China	86.90	48.03	MW172532	This study

E. dzungarica	Guo3100	♀	62	Hap 5	Baishashan desert, Habahe County, Xinjiang, China	86.90	48.03	MW172533	This study
E. szczerbaki	ZMMU R-14342-1	\	1	Hap 46	Naryn Prov., Naryn Distr., N from Naryn, Kyrgyzstan	75.98	41.48	KY366618	Orlova et al. (2017)
E. szczerbaki	ZMMU R-14342-2	\	1	Hap 47	Naryn Prov., Naryn Distr., N from Naryn, Kyrgyzstan	75.98	41.48	KY366619	Orlova et al. (2017)
E. stummeri	ZMMU R-14341-2	\	2	Hap 44	Naryn Prov., Kochkor Distr., S from Kochkor, Kyrgyzstan	75.66	42.08	KY366616	Orlova et al. (2017)
E. stummeri	ZMMU R-14341-3	\	2	Hap 45	Naryn Prov., Kochkor Distr., S from Kochkor, Kyrgyzstan	75.66	42.08	KY366617	Orlova et al. (2017)
E. stummeri	ZMMU R-14339-1	\	3	Hap 41	Naryn Prov., Kochkor Distr., Kochkor, Kyrgyzstan	75.75	42.22	KY366615	Orlova et al. (2017)
E. stummeri	ZMMU R-12556-1	\	4	Hap 37	Issyk-Kul Prov., env. of Balykchy, road to Akolen, Kyrgyzstan	76.17	42.35	KY366611	Orlova et al. (2017)
E. stummeri	ZMMU R-12556-2	\	4	Hap 37	Issyk-Kul Prov., env. of Balykchy, road to Akolen, Kyrgyzstan	76.17	42.35	KY366612	Orlova et al. (2017)
E. stummeri	ZMMU R-12557-1	\	4	Hap 43	Issyk-Kul Prov., env. of Balykchy, road to Akolen, Kyrgyzstan	76.17	42.35	KY366613	Orlova et al. (2017)
E. stummeri	ZMMU R-12557-2	\	4	Hap 43	Issyk-Kul Prov., env. of Balykchy, road to Akolen, Kyrgyzstan	76.17	42.35	KY366614	Orlova et al. (2017)
E. stummeri	ZMMU R-12427-1	\	5	Hap 42	Issyk-Ku1 Prov., NW bank of issyk-Kul lake, 20-25 km N from Toru Aygyr, Kungei-Alatau Mts., Kyrgyzstan	76.41	42.58	KY366609	Orlova et al. (2017)
E. stummeri	ZMMU R-12427-2	\	5	Hap 42	Issyk-Ku1 Prov., NW bank of issyk-Kul lake, 20-25 km N from Toru Aygyr, Kungei-Alatau Mts., Kyrgyzstan	76.41	42.58	KY366610	Orlova et al. (2017)
E. stummeri	ZMMU R-14338-1	\	6	Hap 41	Issyk-Kul Prov., 100 km SW from Karakol,	77.18	42.16	KY366607	Orlova et al. (2017)

					Kaji-Say env., Kyrgyzstan				
E. stummeri	ZMMU R-14338-2	\	6	Hap 41	Issyk-Kul Prov., 100 km SW from Karakol, Kaji-Say env., Kyrgyzstan	77.18	42.16	KY366608	Orlova et al. (2017)
E. stummeri	ZMMU R-14335-2	\	7	Hap 39	Issyk-Ku1 Prov., E bank of issyk-Kul lake, env. Of Karakol, Kyrgyzstan	78.36	42.46	KY366604	Orlova et al. (2017)
E. stummeri	ZMMU R-14335-3	\	7	Hap 40	Issyk-Ku1 Prov., E bank of issyk-Kul lake, env. Of Karakol, Kyrgyzstan	78.36	42.46	KY366605	Orlova et al. (2017)
E. stummeri	ZMMU R-14335-4	\	7	Hap 40	Issyk-Ku1 Prov., E bank of issyk-Kul lake, env. Of Karakol, Kyrgyzstan	78.36	42.46	KY366606	Orlova et al. (2017)
E. stummeri	ZMMU R-12551-1a	\	8	Hap 34	Almaty Prov., Rayimbek Distr., Ketmen Mts. Foothills, 7-8 km E from Kegen, Kazakhstan	79.32	42.97	KY366589	Orlova et al. (2017)
E. stummeri	ZMMU R-12551-2	\	8	Hap 35	Almaty Prov., Rayimbek Distr., Ketmen Mts. Foothills, 7-8 km E from Kegen, Kazakhstan	79.32	42.97	KY366590	Orlova et al. (2017)
E. stummeri	ZMMU R-12551-2a	\	8	Hap 34	Almaty Prov., Rayimbek Distr., Ketmen Mts. Foothills, 7-8 km E from Kegen	79.32	42.97	KY366591	Orlova et al. (2017)
E. stummeri	ZMMU R-12551-3	\	8	Hap 36	Almaty Prov., Rayimbek Distr., Ketmen Mts. Foothills, 7-8 km E from Kegen, Kazakhstan	79.32	42.97	KY366592	Orlova et al. (2017)
E. stummeri	ZMMU R-12551-4	\	8	Hap 34	Almaty Prov., Rayimbek Distr., Ketmen Mts. Foothills, 7-8 km E from Kegen, Kazakhstan	79.32	42.97	KY366593	Orlova et al. (2017)
E. stummeri	ZMMU R-12551-5	\	8	Hap 34	Almaty Prov., Rayimbek Distr., Ketmen Mts. Foothills, 7-8 km E from Kegen, Kazakhsan	79.32	42.97	KY366594	Orlova et al. (2017)
E. stummeri	ZMMU R-12551-5a	\	8	Hap 34	Almaty Prov., Rayimbek Distr., Ketmen Mts. Foothills, 7-8 km E from Kegen, Kazakhstan	79.32	42.97	KY366595	Orlova et al. (2017)
E. stummeri	ZMMU R-12551-6	\	8	Hap 34	Almaty Prov., Rayimbek Distr., Ketmen Mts. Foothills, 7-8 km E from Kegen, Kazakhsan	79.32	42.97	KY366596	Orlova et al. (2017)
E. stummeri	ZMMU R-12551-7	\	8	Hap 34	Almaty Prov., Rayimbek Distr., Ketmen Mts.	79.32	42.97	KY366597	Orlova et al. (2017)

					Foothills, 7-8 km E from Kegen, Kazakhsan				
E. stummeri	ZMMU R-12551-8	\	8	Hap 34	Almaty Prov., Rayimbek Distr., Ketmen Mts. Foothills, 7-8 km E from Kegen, Kazakhsan	79.32	42.97	KY366598	Orlova et al. (2017)
E. stummeri	ZMMU R-12551-10	\	8	Hap 34	Almaty Prov., Rayimbek Distr., Ketmen Mts. Foothills, 7-8 km E from Kegen, Kazakhsan	79.32	42.97	KY366599	Orlova et al. (2017)
E. stummeri	ZMMU R-1 2495-1	\	8	Hap 37	Almaty Prov., Rayimbek Distr., Ketmen Mts. Foothills, 7-8 km E from Kegen, Kazakhsan	79.32	42.97	KY366600	Orlova et al. (2017)
E. stummeri	ZMMU R-12552-1	\	9	Hap 38	Almaty Prov., Rayimbek Distr., central Tian Shan Mts., 15 km S from Tuzkol Lake, Zhabyrtau Mt., Kazakhstan	80.08	42.92	KY366601	Orlova et al. (2017)
E. stummeri	ZMMU R-12552-2	\	9	Hap 38	Almaty Prov., Rayimbek Distr., central Tian Shan Mts., 15 km S from Tuzkol Lake, Zhabyrtau Mt., Kazakhstan	80.08	42.92	KY366602	Orlova et al. (2017)
E. stummeri	ZMMU R-12552-4	\	9	Hap 38	Almaty Prov., Rayimbek Distr., central Tian Shan Mts., 15 km S from Tuzkol Lake, Zhabyrtau Mt., Kazakhstan	80.08	42.92	KY366603	Orlova et al. (2017)
Eremias sp. 1	ZMMU R-14329-1	\	10	Hap 50	Xinjiang Prov., 60 km NE rrom Aksu, China	80.79	41.54	KY366626	Orlova et al. (2017)
Eremias sp. 1	ZMMU R-14330-1	\	11	Hap 51	Xinjiang Prov., 75 km NE from Aksu, China	80.83	41.74	KY366627	Orlova et al. (2017)
Eremias sp. 1	ZMMU R-14330-2	\	11	Hap 52	Xinjiang Prov., 75 km NE from Aksu, China	80.83	41.74	KY366628	Orlova et al. (2017)
Eremias sp. 1	ZMMU R-14330-3	\	11	Hap 53	Xinjiang Prov., 75 km NE from Aksu, China	80.83	41.74	KY366629	Orlova et al. (2017)
Eremias sp. 1	ZMMU R-14327-1	\	12	Hap 49	Xinjiang Prov., 35 km NE rrom Aksu, China	81.05	41.40	KY366625	Orlova et al. (2017)
Eremias sp. 1	ZMMU R-14328-1	\	13	Hap 54	Xinjiang Prov., 89 km NE from Aksu, China	81.21	41.56	KY366630	Orlova et al. (2017)
Eremias sp. 1	ZMMU R-14328-2	\	13	Hap 55	Xinjiang Prov., 89 km NE from Aksu, China	81.21	41.56	KY366631	Orlova et al. (2017)
Eremias sp. 1	ZMMU R-14328-3	\	13	Hap 56	Xinjiang Prov., 89 km NE from Aksu, China	81.21	41.56	KY366632	Orlova et al. (2017)

E. yarkandensis	ZMMU R-14344-1	\	14	Hap 48	Osh Prov., vicinity of Nura, Kyrgyzstan	73.87	39.65	KY366620	Orlova et al. (2017)
E. yarkandensis	ZMMU R-14344-2	\	14	Hap 48	Osh Prov., vicinity of Nura, Kyrgyzstan	73.87	39.65	KY366621	Orlova et al. (2017)
E. yarkandensis	ZMMU R-14344-3	\	14	Hap 48	Osh Prov., vicinity of Nura, Kyrgyzstan	73.87	39.65	KY366622	Orlova et al. (2017)
E. yarkandensis	ZMMU R-14344-4	\	14	Hap 48	Osh Prov., vicinity of Nura, Kyrgyzstan	73.87	39.65	KY366623	Orlova et al. (2017)
E. yarkandensis	ZMMU R-14344-5	\	14	Hap 48	Osh Prov., vicinity of Nura, Kyrgyzstan	73.87	39.65	KY366624	Orlova et al. (2017)
E. cf. *buechneri*	ZMMU R-8910-1a	\	15	Hap 28	Xinjiang Prov., Qarqan (Chemo) Distr., Altintag Mt., Chinbulak, 60 km S from Turav, China	86.05	37.51	KY366574	Orlova et al. (2017)
E. cf. *buechneri*	ZMMU R-8910-1b	\	15	Hap 28	Xinjiang Prov., Qarqan (Chemo) Distr., Altintag Mt., Chinbulak, 60 km S from Turav, China	86.05	37.51	KY366575	Orlova et al. (2017)
Eremias sp. 2	\	\	16	Hap 26	Qinhai Prov., Delingha env., China	97.35	37.35	KY366572	Orlova et al. (2017)
Eremias sp. 2	\	\	17	Hap 27	Qinhai Prov., Gonghe (Qiabugia), Chekhou, env. Of Kyiking (Chin-Kon), China	100.75	36.20	KY366573	Orlova et al. (2017)
E. cf. *multiocellata*	\	\	18	Hap 65	Gansu Prov., env. of Shandan, China			KY366641	Orlova et al. (2017)
E. przewalskii	ZMMU R-13209	\	19	Hap 17	Inner Mongolia Prov., 30 km W from Bayanhot	101.27	39.12	KY366551	Orlova et al. (2017)
E. przewalskii	\	\	20	Hap 16	Gansu Prov., Minqin County, Wuwei, China	103.11	38.63	KM507330	Orlova et al. (2017)
E. przewalskii	ZMMU R-13214	\	21	Hap 18	Inner Mongolia Prov., Alashan desert, 150 km W from Bayanmod, China	105.59	40.41	KY366552	Orlova et al. (2017)
E. przewalskii	ZMMU R-12046-1	\	22	Hap 19	Bayankhongor Aimaq, Zhinst, Mongolia	100.21	45.62	KY366553	Orlova et al. (2017)
E. przewalskii	ZMMU R-13038-1	\	23	Hap 19	Govi-Altai Aimaq, Biger valley, Mongolia	97.4	45.73	KY366554	Orlova et al. (2017)
E. przewalskii	ZMMU R-13038-3	\	23	Hap 19	Govi-Altai Aimaq, Biger valley, Mongolia	97.4	45.73	KY366555	Orlova et al. (2017)
E. przewalskii	ZMMU R-13038-4	\	23	Hap 19	Govi-Altai Aimaq, Biger valley, Mongolia	97.4	45.73	KY366556	Orlova et al. (2017)
E. przewalskii	ZMMU R-12842-1	\	24	Hap 19	Govi-Aitai Aimaq, 3 km W from Biger Sum, Mongolia	97.15	45.72	KY366557	Orlova et al. (2017)

E. przewalskii	ZMMU R-12842-2	\	24	Hap 19	Govi-Aitai Aimaq, 3 km W from Biger Sum, Mongolia	97.15	45.72	KY366558	Orlova et al. (2017)
E. przewalskii	ZMMU R-12888-1	\	25	Hap 20	Govi-Aitai Aimaq, Tsogt, Dzahuin-Govi, 10 km W Bayan-Toroo, Mongolia	96.65	45.67	KY366559	Orlova et al. (2017)
E. przewalskii	ZMMU R-12888-2	\	25	Hap 20	Govi-Aitai Aimaq, Tsogt, Dzahuin-Govi, 10 km W Bayan-Toroo, Mongolia	96.65	45.67	KY366560	Orlova et al. (2017)
E. przewalskii	ZMMU R-13060-1	\	26	Hap 19	Tuva Republic, Ovyurskiy Distr., Tere-Khollake, Tsuger-Els sands, Russia	93.21	50.68	KY366561	Orlova et al. (2017)
E. przewalskii	ZMMU R-13060-2	\	26	Hap 19	Tuva Republic, Ovyurskiy Distr., Tere-Khollake, Tsuger-Els sands, Russia	93.21	50.68	KY366562	Orlova et al. (2017)
E. przewalskii	ZMMU R-13060-3	\	26	Hap 19	Tuva Republic, Ovyurskiy Distr., Tere-Khollake, Tsuger-Els sands, Russia	93.21	50.68	KY366563	Orlova et al. (2017)
E. przewalskii	ENS-T07-1	\	26	Hap 19	Tuva Republic, Ovyurskiy Distr., Tere-Khollake, Tsuger-Els sands, Russia	93.21	50.68	KY366564	Orlova et al. (2017)
E. przewalskii	ENS-T07-2	\	26	Hap 19	Tuva Republic, Ovyurskiy Distr., Tere-Khollake, Tsuger-Els sands, Russia	93.21	50.68	KY366565	Orlova et al. (2017)
E. cf. *reticulata*	ZMMU R-12855-1	\	27	Hap 22	Gobi-Altai Aimaq, 4 km NW from Altai Sum, env. Danshig-Khuduk, Mongolia	95.86	44.64	KY366567	Orlova et al. (2017)
E. cf. *reticulata*	ZMMU R-12855-2	\	27	Hap 23	Gobi-Altai Aimaq, 4 km NW from Altai Sum, env. Danshig-Khuduk, Mongolia	95.86	44.64	KY366568	Orlova et al. (2017)
E. cf. *reticulata*	ZMMU R-12856-1	\	27	Hap 23	Gobi-Altai Aimaq, 4 km NW from Altai Sum, env. Danshig-Khuduk, Mongolia	95.86	44.64	KY366569	Orlova et al. (2017)
E. cf. *reticulata*	MNUE-Em-S	\	28	Hap 21	Bayankhongor Aimaq, Tsagan Bogdo Uul (Mt.)	98.82	42.88	KY366566	Orlova et al. (2017)
E. cf. *przewalskii*	ZMMU R-12858-1	\	29	Hap 24	ömnögovi Aimaq, 8-10 km S from Bayandalai Sum, Mongolia	103.45	43.39	KY366570	Orlova et al. (2017)
E. cf. *przewalskii*	ZMMU R-12859-1	\	29	Hap 25	ömnögovi Aimaq, 8-10 km S from Bayandalai	103.45	43.39	KY366571	Orlova et al. (2017)

					Sum, Mongolia				
Eremias sp. 3	\	\	30	Hap 64	Gansu Prov., env. of Lanzhou, Baiyin, China	104.21	36.46	KJ664798	Li and Song (unpublished data)
Eremias sp. 3	\	\	31	Hap 63	Gansu Prov., Minqin County, China	103.11	38.63	NC025304	Tong et al. (2014)
Eremias sp. 3	ZMMU R-13208	\	32	Hap 62	Inner Mongolia Prov., 80 km SW Sayan Nur, China	103.87	40.00	KY366640	Orlova et al. (2017)
Eremias sp. 3	ZMMU R-13207	\	33	Hap 60	Inner Mongolia Prov., 120 km W from Wuhai, China	105.45	39.53	KY366638	Orlova et al. (2017)
Eremias sp. 3	ZMMUR-13206	\	34	Hap 61	Inner Mongolia Prov., Alashan desert, 40 km S from Bayan-Hot, China	105.62	38.67	KY366639	Orlova et al. (2017)
Eremias sp. 3	ZMMU R-13205	\	35	Hap 59	Inner Mongolia Prov., W Ordos, 30 km SW from Bayan-Us, China	108.50	40.02	KY366637	Orlova et al. (2017)
Eremias sp. 3	ZMMU R-13215	\	36	Hap 58	Inner Mongolia Prov., 50 km S from Baotou, China	110.00	40.28	KY366636	Orlova et al. (2017)
Eremias sp. 3	ZMMU R-12610-1a	\	37	Hap 57	Dornogovi Aimaq, Sainshand Sum, vicinity of Saishand, Mongolia	110.10	44.89	KY366633	Orlova et al. (2017)
Eremias sp. 3	ZMMU R-12610-1b	\	37	Hap 57	Dornogovi Aimaq, Sainshand Sum, vicinity of Saishand, Mongolia	110.10	44.89	KY366634	Orlova et al. (2017)
Eremias sp. 3	ZMMU R-14523	\	38	Hap 57	Dornogovi Aimaq, Sainshand Sum, ca. 100 km NE from örgön, Mongolia	111.79	45.18	KY366635	Orlova et al. (2017)
E. multiocellata	ZMMU R-12863-1	\	39	Hap 72	Umnugovi Aimaq, 102 km NW from Dalandzadagat, Tsogt-Ovu, Mongolia	105.32	44.42	KY366651	Orlova et al. (2017)
E. multiocellata	ZMMU R-12863-2	\	39	Hap 73	Umnugovi Aimaq, 102 km NW from Dalandzadagat, Tsogt-Ovu, Mongolia	105.32	44.42	KY366652	Orlova et al. (2017)
E. multiocellata	ZMMU R-12952a	\	40	Hap 70	Dundgovi Aimaq, env. of Deren, Mongolia	106.54	46.59	KY366647	Orlova et al. (2017)

E. multiocellata	ZMMU R-12952b	\	40	Hap 70	Dundgovi Aimaq, env. of Deren, Mongolia	106.54	46.59	KY366648	Orlova et al. (2017)
E. multiocellata	ZMMU R-12608-1	\	41	Hap 71	Dundgovi Aimaq, env. of ölziit Sum, Mongolia	102.51	48.03	KY366649	Orlova et al. (2017)
E. multiocellata	ZMMU R-12608-2	\	41	Hap 71	Dundgovi Aimaq, env. of ölziit Sum, Mongolia	102.51	48.03	KY366650	Orlova et al. (2017)
E. multiocellata	ZMMU R-12045-1	\	42	Hap 74	Bayankhongor Aimaq, Zhinst, Mongolia	100.21	45.62	KY366653	Orlova et al. (2017)
E. multiocellata	ZMMU R-12045-2	\	42	Hap 74	Bayankhongor Aimaq, Zhinst, Mongolia	100.21	45.62	KY366654	Orlova et al. (2017)
E. multiocellata	ZMMU R-12841-1	\	43	Hap 74	Bayankhongor Aimaq, N bank of Böönтsagan Nuur Lake, Mongolia	99.12	45.67	KY366655	Orlova et al. (2017)
E. multiocellata	ZMMU R-12841-2	\	43	Hap 74	Bayankhongor Aimaq, N bank of Böönтsagan Nuur Lake, Mongolia	99.12	45.67	KY366656	Orlova et al. (2017)
E. multiocellata	ZMMU R-13039-1	\	44	Hap 74	Govi-Altai Aimaq, Delger, Mongolia	98.05	45.93	KY366657	Orlova et al. (2017)
E. multiocellata	ZMMU R-12843-1	\	45	Hap 75	Govi-Altai Aimaq, Shargyn-Govi, 2 km SW from Khalium Sum, Mongolia	96.12	45.93	KY366658	Orlova et al. (2017)
E. multiocellata	ZMMU R-12843-2	\	45	Hap 75	Govi-Altai Aimaq, Shargyn-Govi, 2 km SW from Khalium Sum, Mongolia	96.12	45.93	KY366659	Orlova et al. (2017)
E. multiocellata	ZMMU R-12081-1	\	46	Hap 76	Govi-Aitai Aimaq, Shargyn-Govi, 30 km S from Sharga Sum, Mongolia	95.23	46.36	KY366660	Orlova et al. (2017)
E. multiocellata	ZMMU R-13058-1	\	47	Hap 66	Tuva Republic, Erzin Distr., Ubsu-Nw valley， 12 km SE from Yamalyg Mt. , Russia	94.79	50.16	KY366642	Orlova et al. (2017)
E. multiocellata	ZMMU R-13058-2	\	47	Hap 67	Tuva Republic, Erzin Distr., Ubsu-Nw valley， 12 km SE from Yamalyg Mt., Russia	94.79	50.16	KY366643	Orlova et al. (2017)
E. multiocellata	ZMMU R-13058-3	\	47	Hap 68	Tuva Republic, Erzin Distr., Ubsu-Nw valley， 12 km SE from Yamalyg Mt., Russia	94.79	50.16	KY366644	Orlova et al. (2017)
E. multiocellata	ZMMU R-13058-4	\	47	Hap 69	Tuva Republic, Erzin Distr., Ubsu-Nw valley， 12 km SE from Yamalyg Mt., Russia	94.79	50.16	KY366645	Orlova et al. (2017)

E. multiocellata	ZMMU R-13059-1	\	47	Hap 67	Tuva Republic, Erzin Distr., Ubsu-Nw valley, 12 km SE from Yamalyg Mt., Russia	94.79	50.16	KY366646	Orlova et al. (2017)
E. multiocellata	ZMMU R-12844-1	\	48	Hap 74	Govi-Aitai Aimaq, Junggar Govi, 4 km W from Bidzh, Mongolia	93.58	45.59	KY366661	Orlova et al. (2017)
E. multiocellata	ZMMU R-12844-2	\	48	Hap 74	Govi-Aitai Aimaq, Junggar Govi, 4 km W from Bidzh, Mongolia	93.58	45.59	KY366662	Orlova et al. (2017)
E. multiocellata	ZMMU R-12853-1	\	49	Hap 74	Govi-Aitai Aimaq, Junggar Govi, Bugat, Mongolia	93.53	45.22	KY366663	Orlova et al. (2017)
E. multiocellata	ZMMU R-12853-2	\	49	Hap 74	Govi-Aitai Aimaq, Junggar Govi, Bugat, Mongolia	93.53	45.22	KY366664	Orlova et al. (2017)
E. multiocellata	ZMMU R-12848-1	\	50	Hap 74	Khovd Aimaq, 58 km SE from Altai Sum, E foothills of Sertengiyn-Khuvch-Ula, Mongolia	92.98	45.65	KY366665	Orlova et al. (2017)
E. multiocellata	ZMMU R-12849-1	\	50	Hap 77	Khovd Aimaq, 58 km SE from Altai Sum, E foothills of Sertengiyn-Khuvch-Ula, Mongolia	92.98	45.65	KY366666	Orlova et al. (2017)
E. multiocellata	ZMMU R-12849-2	\	50	Hap 74	Khovd Aimaq, 58 km SE from Altai Sum, E foothills of Sertengiyn-Khuvch-Ula, Mongolia	92.98	45.65	KY366667	Orlova et al. (2017)
E. multiocellata	ZMMU R-12847-1	\	51	Hap 75	Khovd Aimaq, I km SW from Altai Sum, Mongolia	92.25	45.80	KY366668	Orlova et al. (2017)
E. multiocellata	ZMMU R-13132-1	\	52	Hap 74	Khovd Aimaq, 7 km SW from Uyench Sum, Mongolia	93.61	46.93	KY366669	Orlova et al. (2017)
E. multiocellata	ZMMU R-13132-2	\	52	Hap 74	Khovd Aimaq, 7 km SW from Uyench Sum, Mongolia	93.61	46.93	KY366670	Orlova et al. (2017)
E. multiocellata	ZMMU R-13132-3	\	52	Hap 74	Khovd Aimaq, 7 km SW from Uyench Sum, Mongolia	93.61	46.93	KY366671	Orlova et al. (2017)
E. multiocellata	ZMMU R-13132-4	\	52	Hap 74	Khovd Aimaq, 7 km SW from Uyench Sum, Mongolia	93.61	46.93	KY366672	Orlova et al. (2017)
E. multiocellata	ZMMU R-13132-5	\	52	Hap 74	Khovd Aimaq, 7 km SW from Uyench Sum, Mongolia	93.61	46.93	KY366673	Orlova et al. (2017)

E. dzungarica	ZMMU R-12845-2	\	52	Hap 31	Khovd Aimaq, 7 km SW from Uyench Sum, Mongolia	93.61	46.93	KY366580	Orlova et al. (2017)
E. dzungarica	ZMMU R-12845-4	\	52	Hap 31	Khovd Aimaq, 7 km SW from Uyench Sum, Mongolia	93.61	46.93	KY366581	Orlova et al. (2017)
E. dzungarica	ZMMU R-12845-5	\	52	Hap 32	Khovd Aimaq, 7 km SW from Uyench Sum, Mongolia	93.61	46.93	KY366582	Orlova et al. (2017)
E. dzungarica	ZMMU R-12845-6	\	52	Hap 31	Khovd Aimaq, 7 km SW from Uyench Sum, Mongolia	93.61	46.93	KY366583	Orlova et al. (2017)
E. dzungarica	ZMMU R-12845-7	\	52	Hap 31	Khovd Aimaq, 7 km SW from Uyench Sum, Mongolia	93.61	46.93	KY366584	Orlova et al. (2017)
E. dzungarica	ZMMU R-12845-8	\	52	Hap 31	Khovd Aimaq, 7 km SW from Uyench Sum, Mongolia	93.61	46.93	KY366585	Orlova et al. (2017)
E. dzungarica	ZMMU R-12845-9	\	52	Hap 31	Khovd Aimaq, 7 km SW from Uyench Sum, Mongolia	93.61	46.93	KY366586	Orlova et al. (2017)
E. dzungarica	ZMMU R-12845-10	\	52	Hap 31	Khovd Aimaq, 7 km SW from Uyench Sum, Mongolia	93.61	46.93	KY366587	Orlova et al. (2017)
E. dzungarica	ZMMU R-12862-1	\	53	Hap 31	Khovd Aimaq, Bulgan Sum, Bayan-Mod, 11 km W from Ikher-Toli, Mongolia	92.91	47.06	KY366578	Orlova et al. (2017)
E. dzungarica	ZMMU R-12862-3	\	53	Hap 31	Khovd Aimaq, Bulgan Sum, Bayan-Mod, 11 km W from Ikher-Toli, Mongolia	92.91	47.06	KY366579	Orlova et al. (2017)
E. dzungarica	ZMMU R-12550-1	\	54	Hap 33	Khovd Aimaq, 24 km N from Uyench Sum, Mongolia	92.05	46.27	KY366588	Orlova et al. (2017)
E. dzungarica	ZMMU R-11989-1	\	55	Hap 29	East-Kazakhstan Prov., Aigyrkum sands, 5-7 km SW from Buran	84.89	47.98	KY366576	Orlova et al. (2017)
E. dzungarica	ZMMU R-11989-2	\	55	Hap 30	East-Kazakhstan Prov., Aigyrkum sands, 5-7 km SW from Buran	84.89	47.98	KY366577	Orlova et al. (2017)

E. argus barbouri	ZMMU R-12605-1	\	\	\	\	\	\	KY366548	Orlova et al. (2017)
E. brenchleyi	\	\	\	\	Qianshan, Suzhou, Anhui Province, China	\	\	EF490071	Rui et al. (2009)
E. nikolskii	ZMMU R-11673-1	\	\	\	\		\	KY366550	Orlova et al. (2017)
E. vermiculata	ZMMU-R12047-1	\	\	\	\	\	\	KY366549	Orlova et al. (2017)

References

Orlova VF, Poyarkov Jr NA, Chirikova MA, Nazarov RA, Munkhbaatar M, Munkhbayar K, Terbish K. 2017. MtDNA differentiation and taxonomy of Central Asian racerunners of *Eremias multiocellata-E. przewalskii* species complex (Squamata, Lacertidae). *Zootaxa*, **4282**(1): 1−42.

Rui J, Wang Y, Nie L. 2009. The complete mitochondrial DNA genome of *Eremias brenchleyi* (Reptilia: Lacertidae) and its phylogeny position within squamata reptiles. *Amphibia-Reptilia*, **30**: 25-35

Supplementary Table S2 Kimura 2-parameter (K2P) distance summary for sequence divergence between barcoding mitochondrial *COI* sequences at species and genus level

	Individuals	Taxa	Comparisons	Min%	Mean%	Max%	SE%
Within species	155	12	2018	0.00	1.16	6.18	0.00
Within genus	156	1	10072	0.77	9.09	13.19	0.00

Supplementary Table S3 Kimura 2-parameter (K2P) distance summary of maximum intraspecific variation and minimum genetic distance to the nearest-neighbor species calculated from barcoding mitochondrial *COI* sequences for each species in *Eremias multiocellata-przewalskii* species complex

Species	Max Intra-Sp (%)	Nearest Species	Distance to NN (%)
Eremias sp. 2	0.31	*Eremias*. cf. *reticulata*	0.77
Eremias. cf. *reticulata*	0.31	*Eremias* sp. 2	0.77
Eremias przewalskii	2.19	*Eremias*. cf. *przewalskii*	1.08
Eremias. cf. *przewalskii*	0.31	*Eremias przewalskii*	1.08
Eremias cf. *buechneri*	0	*Eremias yarkandensis*	1.48
Eremias yarkandensis	0	*Eremias* cf. *buechneri*	1.48
Eremias. dzungarica	2.99	*Eremias* cf. *buechneri*	1.87
Eremias sp. 1	2.14	*Eremias yarkandensis*	3.35
Eremias multiocellata	1.71	*Eremias* sp. 3	5.65
Eremias sp. 3	6.18	*Eremias multiocellata*	5.65
Eremias cf. *multiocellata*	N/A	*Eremias multiocellata*	6.85
Eremias stummeri	2.47	*Eremias szczerbaki*	7.58
Eremias szczerbaki	0.33	*Eremias stummeri*	7.58

Supplementary Table S4 Quantitative characteristics of specimens of *Eremias dzungarica* from this study and Orlova et al. (2017)

Values are given as ranges and means ± SE. Morphological characters detected with significant sexual dimorphism are given separately for females and males.

Table S4.1

Metric and meristic traits	Females of *E. dzungarica* in this study			Females of *E. dzungarica* from Orlova et al. (2017)		
	N	Range	Mean ± SE	N	Range	Mean ± SE
SVL	15	46.55-64.46	57.79 ± 1.443	2	61.40-64.50	\
TL	7	63.65-76.19	69.96 ± 1.794	0	\	\
Ga	15	21.48-33.07	28.72 ± 0.941	2	33.80-35.00	\
HL	15	11.59-15.40	13.64 ± 0.279	2	14.00-15.00	\
HW	15	6.99-9.89	8.66 ± 0.196	2	7.00-8.20	\
HH	15	5.47-8.07	6.96 ± 0.215	2	6.00-7.20	\
NL	15	15.98-20.96	18.40 ± 0.353	2	19.00-20.50	\
Pa	15	16.14-20.48	18.68 ± 0.346	2	18.00-19.00	\
Pp	15	23.95-29.66	26.98 ± 0.459	2	25.40-26.20	\
Dist.P.fm	15	3.52-5.42	4.73 ± 0.117	2	1.60-1.70	\
Sq.c.cd	15	24-27	25.13 ± 0.274	2	23-23	
Lpil.	15	10.74-14.15	12.34 ± 0.236	0	\	\

Table S4.2

Metric and meristic traits	Males of *E. dzungarica* in this study			Males of *E. dzungarica* from Orlova et al. (2017)		
	N	Range	Mean ± SE	N	Range	Mean ± SE
SVL	15	56.14-75.72	63.44 ± 1.378	5	52.00-65.00	58.72 ± 2.506
TL	11	72.74-94.82	80.79 ± 2.121	2	67.30-85.00	\
Ga	15	25.23-35.61	31.08 ± 0.853	5	24.00-32.00	28.240 ± 1.574
HL	15	15.10-18.98	16.45 ± 0.343	5	13.60-18.00	15.88 ± 0.779
HW	15	8.82-12.20	10.50 ± 0.232	5	7.30-10.30	9.00 ± 0.640
HH	15	7.16-10.72	8.84 ± 0.272	5	5.00-8.30	6.86 ± 0.616
NL	15	19.53-26.14	21.93 ± 0.473	5	12.50-21.40	18.96 ± 1.688
Pa	15	18.14-24.33	20.81 ± 0.414	5	17.50-20.00	19.20 ± 0.464
Pp	15	26.64-35.41	31.16 ± 0.654	5	25.70-30.00	28.48 ± 0.813
Dist.P.fm	15	3.52-6.34	4.68 ± 0.219	5	1.70-2.50	2.06 ± 0.129
Sq.c.cd	15	25-29	26.67 ± 0.319	5	24-27	25.20 ± 0.583
Lpil.	15	13.26-16.48	14.35 ± 0.270	0	\	\

Table S4.3

Meristic traits	All specimens of *E. dzungarica* in this study			All specimens of *E. dzungarica* from Orlova et al. (2017)		
	N	Range	Mean ± SE	N	Range	Mean ± SE
Lab.total.L	30	9–12	10.83 ± 0.145	11	9–11	10.36 ± 0.203
Lab.total.R	30	9–12	10.60 ± 0.141	11	9–11	10.00 ± 0.234
Infralab.L	30	6–7	6.63 ± 0.089	12	6–8	6.83 ± 0.167
Infralab.R	30	6–8	6.77 ± 0.092	12	6v9	6.92 ± 0.260
Sq.	30	44–55	47.67 ± 0.456	12	46–52	48.42 ± 0.609
Ventr.	30	30–34	31.93 ± 0.185	12	30v32	30.92 ± 0.193
G.	30	20–26	22.93 ± 0.335	12	21–26	22.83 ± 0.474
Coll.	30	9–14	11.27 ± 0.267	11	7–13	11.00 ± 0.632
Lam.subdig.	30	22–25	23.53 ± 0.224	12	19–24	21.58 ± 0.379
P.fm.L	30	10–13	11.17 ± 0.167	12	9–15	12.17 ± 0.405
P.fm.R	30	9–14	11.33 ± 0.188	12	9–14	12.00 ± 0.369
Ventr.long.	30	14–18	16.30 ± 0.199	1	16	\
supracil.L	30	3–8	5.43 ± 0.196	0	\	\
supracil.R	30	4–7	5.47 ± 0.124	0	\	\
scal.f.p	30	7–12	9.70 ± 0.204	0	\	\

Supplementary Table S5 Morphological characters used for morphometric analysis and their corresponding abbreviations

Abbreviations	Description of morphological trait
SVL	Snout to vent length
TL	Tail length
Ga	Gleno-acetobular distance (from axilla to groin)
HL	Head length
HW	Head width
HH	Head height
Lpil.	Pileus Length (from rostrum to the posterior border of parietals)
NL	head length from snout tip to the anterior edge of collar (measured from ventral side)
Pa	Forelimb Length
Pp	Hindlimb Length
Dist.P.fm.	Distance between femoral pore rows
Lab.total.L	Number of supralabials on the left side
Lab.total.R	Number of supralabials on the right side
Infralab.L	Number of infralabials on the left side
Infralab.R	Number of infralabials on the right side
Sq.	Number of scales around middorsal
Ventr.	Number of transverse rows of ventral scales
G.	Number of gular scales along mid-line of throat
Coll.	Number of collar scales
Lam.subdig.	Number of subdigital lamellae on the 4th toe of hindlimb
P.fm.L	Number of femoral pores on the left side
P.fm.R	Number of femoral pores on the right side
Ventr.long.	Maximal number of longitudinal rows of ventral scales
Supracil.L	Number of supraciliary scales on the left side
Supracil.R	Number of supraciliary scales on the right side
Scal.f.p	Number of scales between femoral pore rows
Sq.c.cd.	Number of scales around the 9–10th tail ring